Regulation of BMP and TGFβ signaling pathway in cancer progression

Ren, J.

Citation

Ren, J. (2020, June 24). *Regulation of BMP and TGFβ signaling pathway in cancer progression*. Retrieved from https://hdl.handle.net/1887/123057

Cover Page

Universiteit Leiden

Author: Ren, J.
Title: Regulation of BMP and TGFβ signaling pathway in cancer progression
Issue Date: 2020-06-24

Chapter 3

Cancer-associated Fibroblast-derived Gremlin 1 Promotes Breast Cancer Progression

Jiang Ren, Marcel Smid, Josephine Iaria, Daniela C. F. Salvatori,
Hans van Dam, Hong Jian Zhu, John W.M. Martens and Peter ten Dijke

Abstract

Bone morphogenetic proteins (BMPs) have been reported to maintain epithelial integrity and to antagonize the transforming growth factor β (TGFβ)-induced epithelial to mesenchymal transition. The expression of soluble BMPs antagonists is dysregulated in cancers and interrupts proper BMP signaling in breast cancer. In this study, expression analysis of clinical breast cancer datasets revealed that high expression of *GREM1* in breast cancer stroma is correlated with a poor prognosis regardless of the molecular subtype. The large majority of human breast cancer cell lines did not express *GREM1 in vitro*, but breast CAFs did express *GREM1* both *in vitro* and *in vivo*. Transforming growth factor β (TGFβ) secreted by breast cancer cells, and also inflammatory cytokines, stimulated *GREM1* expression in CAFs. Grem1 abrogated BMP/SMAD signaling in breast cancer cells and promoted their mesenchymal phenotype, stemness and invasion. Moreover, Grem1 production by CAFs strongly promoted the fibrogenic activation of CAFs and promoted breast cancer cell intravasation and extravasation in co-injection xenograft zebrafish models. Our results demonstrated that Grem1 is a pivotal factor in the reciprocal interplay between breast cancer cells and CAFs, which promotes cancer cell invasion. Targeting Grem1 could be beneficial in the treatment of breast cancer patients with high Grem1 expression.

Background

Although carcinomas, which account for approximately 90% of human cancers, are derived from epithelia, the tumor stroma exerts a powerful influence on cancer behavior, such as tumor cell growth, invasion, metastasis and evading immune responses. The tumor stroma consists of cancer-associated fibroblasts (CAFs), vascular, inflammatory and immune cells, and extracellular matrix (ECM) residing within or in the vicinity of a tumor [1]. CAFs are differentiated from quiescent fibroblasts and are associated with increased expression of myofibroblastic markers, such as vimentin, α-smooth muscle actin (αSMA), fibroblast activation protein (FAP) and fibroblast-specific protein 1 (FSP1, also known as S100A4) [2]. Tumors, including those from breast, often display desmoplasia (a fibrillar network) that is mainly caused by CAFs, in that they produce and remodel ECM components, including collagen, fibronectin, and laminin [3]. The increased stiffness and abnormal physical structure of the ECM can promote tumor cell growth and metastatic dissemination and are also critical for the generation and maintenance of the CAF phenotype [3].

Bone morphogenetic proteins (BMPs) are secreted growth factors that belong to the transforming growth factor β (TGFβ) family [4]. Signaling by BMPs is initiated by binding their cognate transmembrane serine/threonine kinase receptors, which triggers the phosphorylation of intracellular SMAD1/5/8 (R-SMADs). Activated R-SMADs can form heteromeric complexes with SMAD4 that accumulate in the nucleus, where they can regulate transcriptional responses in concert with other DNA-binding transcription factors [4]. BMP signaling can elicit diverse and complex biological processes in development and disease, including cancer [5]. Many secreted BMP antagonists, which sequester BMP ligands and prevent their binding to receptors, have been identified [6]. Accumulating evidence indicates that several cancer types show dysregulated BMP signaling caused by a disequilibrium of BMPs and their antagonists. For example, BMP antagonists such as Noggin, Follistatin and Chordin like (Chrdl)1 have been linked to inducing osteoclast differentiation and promoting osteolytic bone metastases [7, 8]. The BMP antagonist Coco permits a few dormant breast cancer cells to escape the quiescent state imposed by BMP signaling and thereby establish metastases [9].

Gremlin (Grem) 1 is a highly conserved glycoprotein belonging to the Cerberus and Dan subfamily of secreted BMP antagonists [10]. It preferentially interacts with BMP2, 4, and 7 [11]. Grem1 is the major BMP antagonist that maintains proper outgrowth and patterning during

vertebral limb development [12]. Grem1 expression is also essential for cellular proliferation and branching morphogenesis in lung development and in kidney organogenesis [12, 13]. Aberrant expression in adults is associated with orofacial clefting [14], osteoarthritis [15], spontaneous bone fractures [16], and liver [17], lung [18], and renal [19] fibrosis. Grem1-mediated proangiogenic and proinflammatory activity appears to be independent of its effects on BMP [20, 21].

In several cancers, Grem1 reduces the negative effect of BMPs on stemness, proliferation, migration and invasion of cancer cells [22-24]. In hereditary mixed polyposis syndrome, *GREM1* is predominantly expressed in the epithelium of the large bowel, where it disrupts homeostatic intestinal morphogen gradients and initiates colonic tumorigenesis [25, 26]. *GREM1* was also detected at the colorectal cancer desmoplastic invasion front, highlighting a potential role in cancer metastasis [27]. High levels of *GREM1* gene expression were observed in the stromal fibroblasts of many types of cancer [23, 28, 29], suggesting that CAFs are a potential source of Grem1. However, the effects of Grem1 on CAFs' function and on the interaction between (breast) cancer cells and fibroblasts are unclear.

The results presented here support the idea that Grem1 is a clinical predictor of a poor prognosis in breast cancer. Mechanistically, Grem1 produced by CAFs promoted fibroblast activation in an autocrine manner and stimulated breast cancer cell stemness and invasion in a paracrine manner. Grem1 could be an attractive therapeutic target to interfere with breast cancer progression.

Methods

Data mining of genes expression in clinical patient samples and 52 breast cancer cell lines

In-house and publicly available gene expression datasets *GSE2034* [30], *GSE5327* [31], *GSE2990* [32], *GSE7390* [33] and *GSE11121* [34] were used for *GREM1* (and *transforming growth factor beta1/2/3* (*TGFB1/2/3*), *interleukin 1 beta* (*IL1B*) and *tumor necrosis factor alpha* (*TNFA*)) expression in lymph node-negative, non-(neo-) adjuvant treated primary breast cancer patients with available metastasis-free survival data, leading to a cohort of 867 patients. Using the GSE41313 dataset [35], *GREM1*, *BMPs* and *BMP receptors* expression was assessed in silico in 52 breast cancer cell lines. Breast cancer dataset *GSE14548* [28] was investigated to explore *GREM1* expression in breast epithelium and stroma; this data set was obtained using tissues from normal breast, grade I, II, III ductal carcinoma *in situ* (DCIS) and invasive breast cancer tissue

that were micro-dissected using a laser capture technique. In addition, the colorectal cancer dataset *GSE39396* [36] was analysed for Grem1 expression; epithelial cells, leukocytes, fibroblasts and endothelial cells were isolated by flow cytometry. Data were gathered from Gene Expression Omnibus (http://www.ncbi.nlm.nih.gov/geo/). Raw.cel files were processed using Frozen robust multiarray analysis (fRMA) parameters (median polish) [37] , after which batch effects were corrected using ComBat [38].

GREM1 RNA *in situ* hybridization (ISH)

A matched breast cancer, adjacent (adenosis or hyperplasia, and cancer free) and adjacent normal tissue microarray (TMA) was purchased from US Biomax (BR724). *GREM1* RNA *in situ* hybridization was conducted with an RNAscope *GREM1* Probe (312831-C2, Advanced Cell Diagnostics) and a 2.5 HD Detection Kit – BROWN (322300, Advanced Cell Diagnostics). All procedures were performed by strictly following the manufacturer's instructions. The ISH results were scanned by a Digital Slide Scanner (Pannoramic 250 Flash III, 3DHISTECH). The presence of intracellular brown punctate dots was considered as positive staining. The signal intensity was scored utilizing a five-point system: 0, no signals visible; 1, weak signals barely visible; 2, visible signals but not intensive; 3, moderate intensive signals; and 4, intensive signals. Scoring was evaluated independently by two observers with similar outcomes.

Cell culture

The human breast cancer cell lines MDA-MB-231 and MCF7 were purchased from ATCC. The human human telomerase reverse transcriptase (hTERT)-immortalized breast CAFs 19TT cells have been previously described [39]. Human foreskin fibroblasts were obtained from Arti A. Ramkisoensing, and have been previously published [40]. These cell lines and human embryonic kidney (HEK) 293T cells were cultured in Dulbecco's modified Eagle's medium (DMEM, 11965092, Thermo Fisher Scientific) supplemented with 10% Fetal Bovine Serum (FBS, 16000044, Thermo Fisher Scientific), 100 U/ml Penicillin/Streptomycin (Pen/Strep, 15140148, Thermo Fisher Scientific). MCF10A (M1) human breast epithelial cell line and MCF10A-derived cell line MCF10A-Ras (M2) were generously provided by Dr. Fred Miller (Barbara Ann Karmanos Cancer Institute, Detroit, USA); both cell lines were cultured in DMEM/F12 medium (11039047, Thermo Fisher Scientific) supplemented with 5% horse serum (26050088, Thermo Fisher Scientific), 20 ng/ml epidermal growth factor (EGF, 01-107, Merck Millipore), 10 mg/ml

insulin (91077C, Sigma-Aldrich), 100 ng/ml cholera enterotoxin (C8052, Sigma-Aldrich), and 0.5 mg/ml hydrocortisone (H0135, Sigma-Aldrich) and 100 U/ml Pen/Strep. Human mesenchymal (HM), W18, W21 fetal mesenchymal stem cells (MSC) were isolated and previously described [40], and cultured in Minimum Essential Medium (MEM) α (32561037, Thermo Fisher Scientific) with 10% FBS, 100 U/ml Pen/Strep. All cell lines were maintained at 37 °C, 5% CO_2, humidified incubator. All fibroblasts and MSCs were routinely cultured in 0.2% gelatin (G9136, Sigma-Aldrich) coated flasks or plates during whole experiment period to avoid possible activation caused by physical rigidity. All cell lines were monthly tested to verify absence of mycoplasma and human cell lines were authenticated by Single nucleotide polymorphism (SNP) analysis.

Plasmids, lentiviral transduction and generation of stable cell lines

The human *GREM1* complementary DNA (cDNA) was cloned from cDNA by PCR and inserted into the pCDH lentiviral vector. pLV-mCherry has been described by our laboratory before [41]. pUltra-Smurf (blue fluorescent protein AmCyan) was obtained from Addgene (48974, Addgene). Human *GREM1* lentiviral shRNAs were obtained from the Sigma MISSION shRNA library. 5 shRNAs were tested, and the two most effective shRNAs TRCN0000063833 (sh#1) and TRCN0000063837 (sh#2) were used.

Lentiviruses were produced by co-transfecting cDNA expression plasmids or shRNAs with helper plasmids pCMV-VSVG, pMDLg-RRE (gag/pol), and pRSV-REV into HEK293T cells using polyethyleneimine (PEI). Cell supernatants were harvested 48 h after transfection and stored at -80°C. MDA-MB-231 and MCF7 cells were labelled with mCherry by infecting for 24 hours (h) with mCherry-expressing lentiviral supernatants diluted 1:1 with normal culture medium in the presence of 5 ng/ml of polybrene (107689, Sigma-Aldrich). 48 h after infection, cells were placed under Neomycin (A1720, Sigma-Aldrich) selection. 19TT and W21 cells were labelled with AmCyan and subjected to positive fluorescence activated cell sorting (FACs). To obtain *GREM1* stable expressing cell lines, M1, M2, MDA-MB-231, W21 cells were infected, and selected with puromycin (P9620, Sigma-Aldrich). Puromycin was used at 1 μg/ml to maintain selection pressure. After infection with *GREM1* targeting shRNAs, 19TT cells were used within short term as 19TT cells are puromycin resistance already.

Stimulation with conditioned medium (CM) or cytokines

72

MDA-MB-231 and MCF7 cells were grown to 70-80% confluency, washed two times with PBS and incubated in serum-free DMEM for 24 h. Conditioned medium (CM) was then collected and passed through a 0.45 mm syringe filter (SLHP033RB, Merck Millipore).

19TT cells were treated with CM, recombinant human TGFβ3 (5 ng/ml, 8420-B3, R&D SYSTEMS and Andrew P. Hinck, University of Pittsburg, USA), interleukin 1β (IL1β, 10 ng/ml, 201-LB, R&D SYSTEMS), or tumor necrosis factor α (TNFα, 10 ng/ml, 210-TA, R&D SYSTEMS) for 1, 3, 6, 12, and 24 h. Buffer-treated controls were used in parallel. For antibody-neutralization assays, TGFβ3 or CM were incubated with control (13C4) or TGFβ (1D11) neutralizing antibody (generously provided by Sanofi Genzyme, Inc.) for 30 minutes (min) before treatment.

For inhibition of BMP signaling by recombinant human Grem1 (rhGrem1, 5190-GR, R&D SYSTEMS), rhGrem1 was pre-incubated with recombinant human BMP2/6 (5 ng/ml, 355-BM/507-BP, R&D SYSTEMS) for 30 min.

Quantitative real-time PCR (qRT-PCR)

Total RNAs were isolated using the NucleoSpin RNA II kit (740955, BIOKE´). A total of 1 μg of RNA was reverse transcribed using the RevertAid First Strand cDNA Synthesis Kit (K1621, ThermoFisher Scientific). Real-time PCR was conducted with GoTaq qPCR Master Mix (A6001, Promega) using CFX Connect Detection System (1855201, Bio-Rad). All target gene expression levels were normalized to *GAPDH*. The sequences of primers used to detect target human genes in qRT-PCR were listed in Table S1.

CAGA-luciferase reporter assay

HEK293T cells were seeded on a 24-well plate at approximately 5×10^4 cells per well. The next day, cells in each well were co-transfected with 0.1μg TGFβ/SMAD-inducible (CAGA)$_{12}$ luciferase transcriptional reporter construct [42] and 0.08 μg β-galactosidase expression construct using PEI. After overnight incubation, cells were starved with serum free medium. 8 h later, serum free media were removed and replaced by CM from breast cancer cell lines. 1 ng/ml TGFβ3 treatment was performed as a standard. After another overnight incubation, luciferase and β-galactosidase activities were measured. The luciferase activity was normalized based on the β-galactosidase activity.

Western blotting

Cells were lysed with RIPA buffer containing 1 × cOmplete Protease Inhibitor Cocktail (11836153001, Roche). Protein concentrations were determined using a bicinchoninic acid protein assay Kit (5000111, Bio-Rad). Proteins were separated by sodium dodecyl sulfate polyacrylamide gel electrophoresis (SDS-PAGE) and transferred onto 45 µm Polyvinylidene difluoride (PVDF) membrane (IPVH00010, Merck Millipore). Membranes were blocked using 5% non-fat dry milk in tris buffered saline with 0.1% Tween 20 (655204, Merck Millipore) and probed with the respective primary and secondary antibodies. The signal was detected using Clarity™ Western ECL Substrate (1705060, Bio-Rad) and ChemiDoc Imaging System (17001402, Bio-Rad). The antibodies used for immunoblotting were raised against the following proteins: phospho-SMAD1/5/8 (pSMAD1/5/8, home-made) [43], αSMA (A2547, Sigma-Aldrich), Fibronectin (F7387, Sigma-Aldrich), FAP (WH0002191M1, Sigma-Aldrich), Collagen I (ab34710, Abcam), Vimentin (5741, Cell signaling), Glyceraldehyde 3-phosphate dehydrogenase (GAPDH, MAB374, Merck Millipore). GAPDH was used as protein loading control.

Flow cytometry

Adherent cells were trypsinized and washed twice with 1% bovine serum albumin (BSA) (A2058, Sigma-Aldrich) in phosphate buffered saline (PBS). The cells were then incubated with fluorescein isothiocyanate (FITC)-conjugated anti-human CD44 (347943, BD Biosciences), R-Phycoerythrin (PE)-conjugated anti-human CD24 (555428, BD Biosciences) antibodies (1:400 dilution) for 30 min at 37 °C in the dark. Fluorescein isothyocianate (FITC)/PE-conjugated IgG isotypes (560952/560951, BD Biosciences) were used as control. Cells were washed twice with 1% BSA in PBS and resuspended in 500 ml of PBS prior to analysis on a FACS Canto flow cytometer (BD Biosciences).

Phalloidin staining

Cells were fixed in 4% formalin, permeabilized with 0.1% Triton X-100, and blocked with 5% BSA (A2058, Sigma-Aldrich) in PBS for 30 min. Then cells were stained with Alexa Fluor 488 Phalloidin (A12379, Thermo Fisher Scientific) to visualize filamentous (F)-actin. The nuclei were stained with 4',6-diamidino-2-fenylindool (DAPI, 62248, Thermo Fisher Scientific). Images were taken by confocal microscopy (SP8, Leica Microsystems).

Mammosphere formation assays

Single-cell suspensions of M1 cells were prepared in DMEM/F12 medium containing 1× B27 (17504044, Thermo Fisher Scientific), 20 ng/ml epidermal growth factor (01-107, Merck Millipore), 20 ng/ml fibroblast growth factors (PHG6015, Thermo Fisher Scientific), and 4 mg/ml heparin (H3149, Sigma-Aldrich). Then, 2000 cells/well were seeded into ultralow attachment 24-well plate (CLS3473-24EA, Corning). After 10 days of standard incubation, the numbers of spheres (> 75 mm diameter) were counted using an inverted microscope (DMi8, Leica Microsystems). For secondary sphere formation, primary spheres were dissociated with Accutase (A1110501, Thermo Fisher Scientific), followed by 25-gauge needles (Z192406, BD Biosciences) mechanically. Next, 2000 cells/well were replated. Sphere-forming efficiency was calculated as the number of spheres (average diameter = 100 μm) formed divided by the number of single cells originally seeded.

Collagen gel contraction assays

The contraction assay [44] was performed to evaluate the contractility of 19TT cells with *GREM1* knockdown or *GREM1*-overexpressing W21 cells. Collagen gels were prepared by mixing fibroblast cell suspensions in serum-free medium and type I collagen (Corning, 354249) solution. The final cell density was 2.0×10^5 cells/ml with 1 mg/ml collagen. A 0.5 ml mixture was cast into each well of a 24-well plate and allowed to polymerize for 30 min at 37 °C. Following gelatinization, another 0.5 ml of serum-free DMEM was added to the gel. Changes of gels were recorded by using a ChemiDoc Imaging System (17001402, Bio-Rad) at a fixed distance above the gels at 24, 48, and 72 h. The surface area of the gels was quantified by ImageJ software. The percentage of contraction was calculated using the formula 100% × (well surface area – gel surface area) / well surface area.

Three-dimensional (3D) spheroid invasion assay

mCherry-labeled MDA-MB-231 or MCF7 cells and co-culture (1:1 mixture) with W21 or 19TT groups were prepared at 1000 cells/ml in complete DMEM. Drops of the single cell suspension (30 μl) were placed onto the lids of 10 cm dishes, which were inverted over dishes containing 10 ml PBS. Hanging drop cultures were incubated 7 days allowing sufficient sedimentation and formation of one spheroid per drop. Images were taken by an inverted fluorescent microscope (DMi8, Leica Microsystems).

The 3D spheroid invasion assay was performed according to our previous study [45] with slight modifications. Single spheroids were embedded in the center of each well of a flat-bottom 96-well plate pre-coated with 50 µl of collagen mixture. Type I collagen (354249, Corning) was neutralized according to the manufacturer's protocol. The collagen mixture was prepared by diluting neutralized collagen with serum-free medium to a final concentration of 2 mg/ml. Eight spheroids generated by each experimental setting were randomly chosen for embedding. After spheroid embedding, another 50 µl of collagen mixture was overlaid onto the collagen matrix in each well. The plate was incubated for 30 min at 37 °C to solidify the gels. Thereafter, 50 µl of serum-free medium was added to each well to prevent the surface from dehydrating. Plates were placed under standard cell culture conditions. Images were taken at days 0, 2 and 4 after embedding by using inverted fluorescence microscopy (DMi8, Leica Microsystems). Invasion was quantified by measuring the area occupied by cells using ImageJ software.

Embryonic zebrafish intravasation and extravasation assay

Zebrafish xenograft breast cancer cell experiments were performed by injecting fluorescently labeled breast cancer cells into embryos at 48 h post-fertilization as described before [41]. Briefly, approximately 400 mCherry-labeled MDA-MB-231 cells were injected into the perivitelline space or the duct of Curvier (DoC) of transgenic zebrafish embryos (*fli* : *enhanced green fluorescent protein (EGFP)*), whose vasculature is marked in green. For co-injection, mCherry-labeled MDA-MB-231 cells and AmCyan-labeled W21 or 19TT cells were mixed at a ratio of 1:1. Then, approximately 400 mixed cells were injected into the zebrafish perivitelline space. Zebrafish embryos were maintained at 34 °C after injection, a compromise for both the fish and the human cell lines. Three days post-injection (dpi) into the perivitelline space, the MDA-MB-231 cells that intravasated from the cell mass toward the embryonic fish body within the head and tail regions were imaged and counted under a confocal microscope (SP5 STED, Leica Microsystems). At 5 dpi into the DoC, the number of MDA-MB-231 cells that extravasated individually from circulation into the collagen fibers of the tail fin or the number of clusters formed by M2 cells collectively was analyzed. At least 200 zebrafish embryos were injected for each condition. After verification by microscopy, only correctly injected and viable zebrafish were used for experimental analysis. All experiments were repeated at least two times independently, and representative experiments are shown.

Statistical analysis

Statistical analyses were performed using GraphPad Prism version 7.0. Numerical data from triplicates are presented as the mean ± standard deviation (s.d.), except for the analysis of zebrafish experiments, where a representative result is expressed as the mean ± standard error (s.e.m). Experiments were analyzed with an unpaired Student's t-test. $P < 0.05$ was considered statistically significant.

Results

High *GREM1* expression in breast tumors is associated with a poor prognosis

BMPs have been reported to maintain epithelial integrity and to antagonize TGFβ-induced epithelial to mesenchymal transition (EMT), an important process for cancer cell invasion and metastasis [5]. Many soluble BMP antagonists have been described to be misexpressed and to interrupt proper BMP signaling in breast cancer [7-9]. We examined the prognostic role of soluble BMP antagonists in primary breast cancer using an in-house and publicly available cohort of 867 untreated lymph node-negative breast cancer patients (see the 'Methods' section for data sets that were used). The median follow-up time of metastasis-free survival (MFS) was 94.1 months (range from 1 to 299.4 months). High expression of *GREM1* was found to be associated with a poor prognosis among all BMP antagonists that were examined. As shown in Figure 1A, according to the *GREM1* mRNA expression level, the subjects were divided evenly into 3 quantiles: low, middle and high. *GREM1* expression was inversely associated with MFS in this cohort, *i.e.,* higher expression, poorer outcome: (low *vs* high: HR (hazard ratio) = 1.35, 95% confidence interval (CI) 1.15-1.57, log rank $P = 0.00018$; low *vs* middle: HR = 1.41, CI 1.02-1.96, $P = 0.036$; middle vs high: HR = 1.31, CI 0.98-1.74, P=0.065). A similar association was observed when dividing subjects into 2 quantiles (Figure S1A). Furthermore, high expression of *GREM1* correlated with a poor prognosis in all the breast cancer molecular subtypes examined: human EGF receptor (HER)2[+], triple[-], estrogen receptor (ER)[+], and ER[-] (Figures S1B-E). Therefore, *GREM1* is a poor prognostic marker of metastasis-free survival in breast cancer regardless of the subtype.

ic*GREM1* is expressed in cancer-associated fibroblasts.

When we examined *GREM1* expression in 52 human breast cancer cell lines by mining previously published datasets (see the 'Methods' section), we found that only 3 breast cancer cell
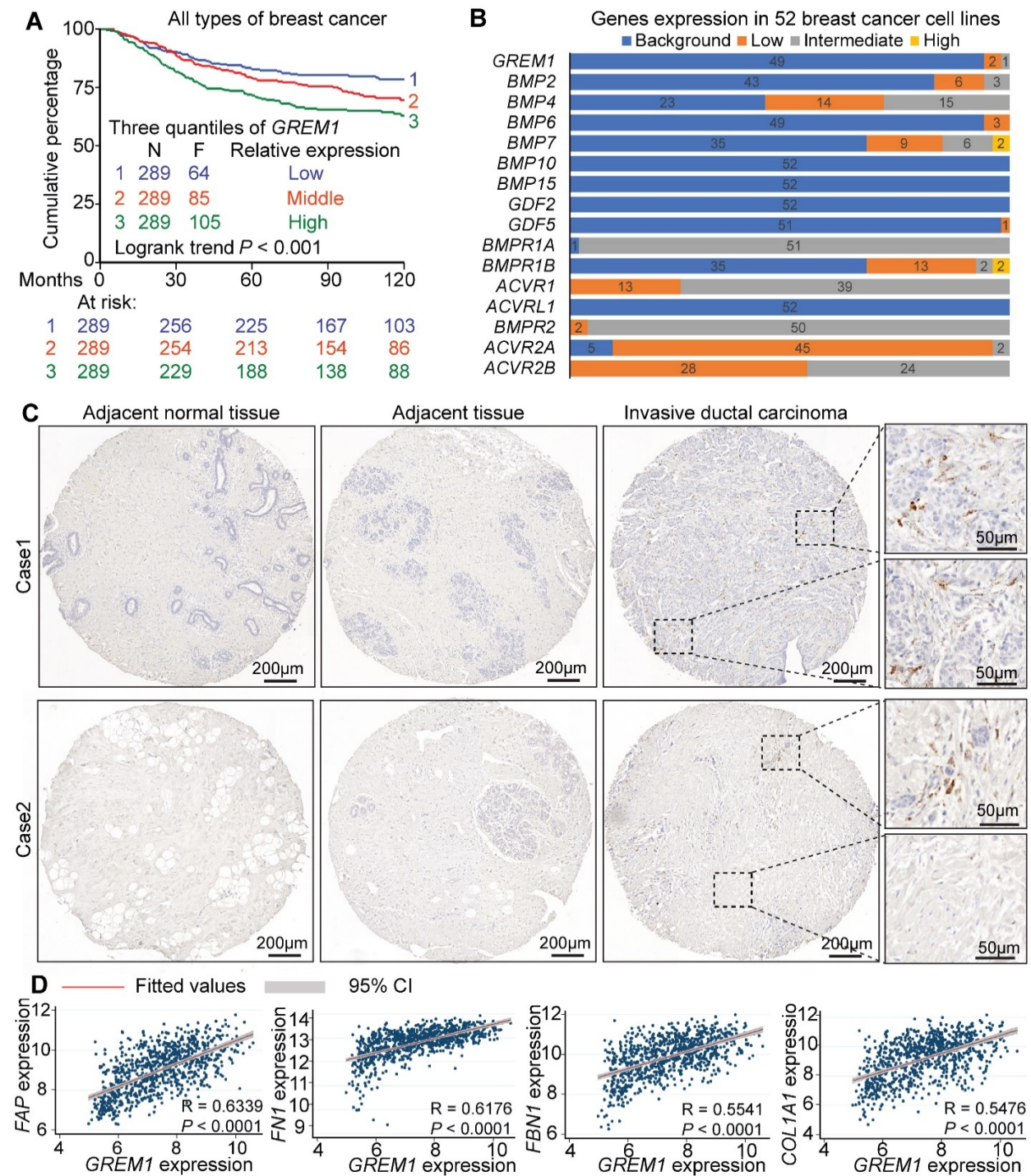
Figure 1. Stromal expression of *GREM1* predicts poor clinical outcome in breast cancer. A, Kaplan-Meier survival curve in untreated lymph node-negative breast cancer patients. Based on *GREM1* mRNA expression (low, middle and high), the subjects (N=867) were divided into 3 quantiles. The endpoint is distant metastasis-free survival. **B**, *GREM1*, *BMPs* and *BMP receptors* mRNA expression level in 52 breast cancer cell lines. The expression levels were categorized to 4 group: Background, Low,

Intermediated, High. **C**, Human *GREM1 in situ* hybridization shows restricted *GREM1* expression in fibroblast-like stromal cells surrounded by malignant breast epithelial cells. **D**, Scatterplot showing positive correlation between the expression of *GREM1* and stromal genes / desmoplastic markers *FAP*, *FN1*, *FBN1*, and *COL1A1* in the clinical datasets. Pearson's coefficient tests were performed to assess statistical significance.

lines express low (MDA-MB-436 and HCC38) or intermediate (SUM149PT) levels of *GREM1*; all other 49 cell lines had no detectable expression (Figure 1B). To explore the source of *GREM1* expression, we stained *GREM1* RNA by using *in situ* hybridization (ISH) in a breast cancer TMA, which comprised 24 matched cases of invasive ductal carcinoma, adjacent tissue and adjacent normal tissue. As shown in Table 1 and Figure 1C, we identified variable amounts of *GREM1* expressed in fibroblast-like cells, *i.e.,* CAFs, whereas there were no detectable levels of *GREM1* in cancer adjacent normal tissues or adjacent cancer free breast tissues. None of the epithelial cells of breast cancers included in this study showed *GREM1*-positive expression. The *GREM1* expression in breast cancer tissue samples is thus mainly caused by the presence of tumor stroma. Moreover, using the in house and publicly available primary breast cancer data sets we observed a significant positive correlation between *GREM1* and markers for CAFs and tumor matrix stiffness/desmoplasia, such as *FAP*, *Fibronectin* (*FN)1*, *Fibrillin* (*FBN)1*, *Collagen (COL)1A1*, *Thrombospondin* (*THBS)2*, and *a-Actin* (*ACTA)2* (Figure 1D, Figure S1F). Taken together, these results suggest that CAF-derived Grem1 might play a pivotal role in promoting breast tumor progression.

Table 1. RNA ISH scores for *GREM1* in matched breast cancer tissue microassay

RNA ISH score	Adjacent normal tissue (%)	Adjacent tissue (%)	Invasive ductal carcinoma (%)
0	24 (100)	24 (100)	4 (16.67)
1	0 (0)	0 (0)	6 (25.00)
2	0 (0)	0 (0)	5 (20.83)
3	0 (0)	0 (0)	5 (20.83)
4	0 (0)	0 (0)	4 (16.67)

TGFβ secreted by cancer cells and inflammatory cytokines induces *GREM1* expression

Analysis of GREM1 in tissue sections revealed that only the CAFs in close proximity to the cancer cells (tumor-stromal interface) showed high *GREM1* RNA expression (Figure 1C, bottom
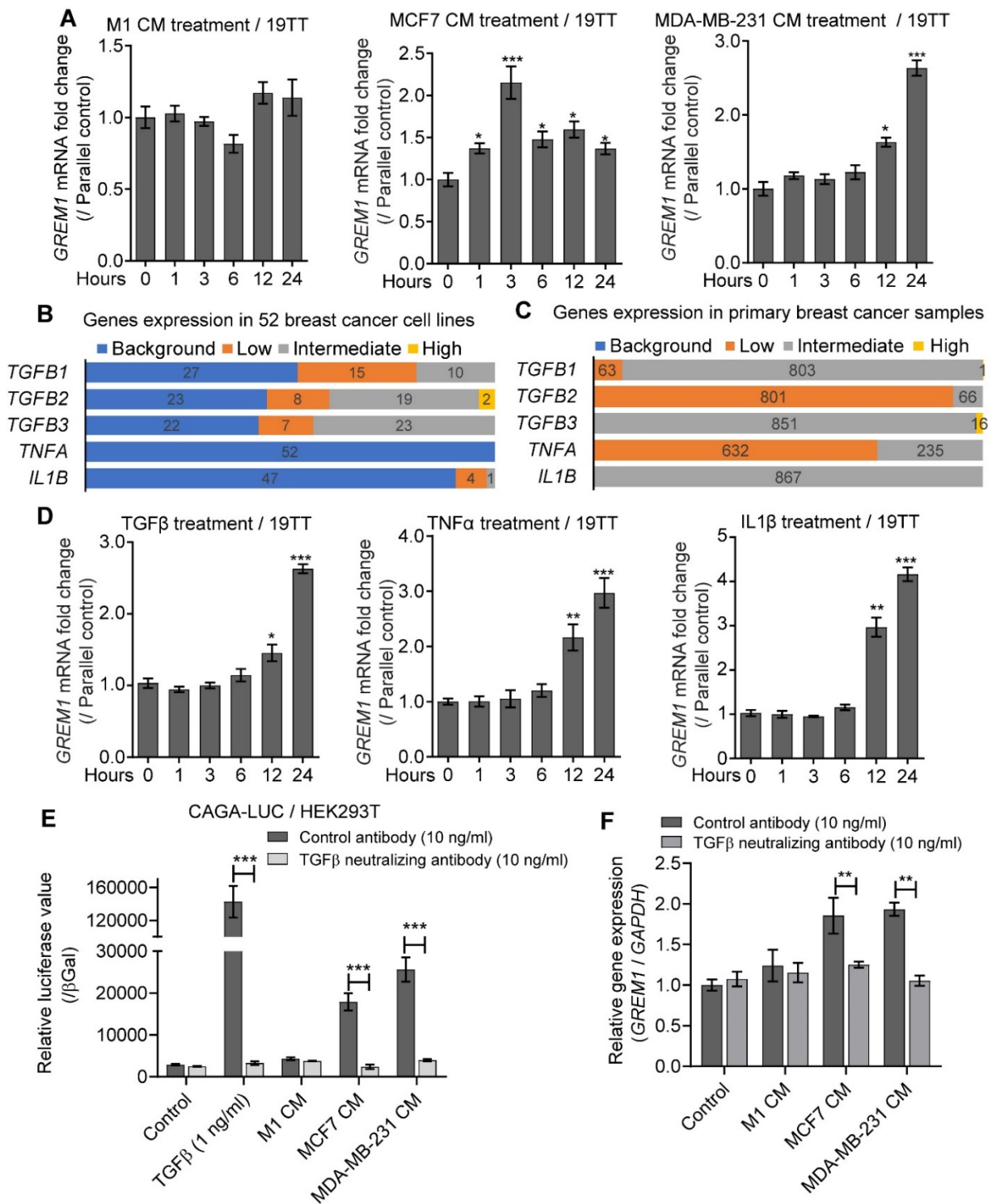
Figure 2. TGFβ secreted by breast cancer cells and inflammatory cytokines induce *GREM1* expression in CAFs. A, *GREM1* expression in 19TT CAFs after treatment with conditioned medium (CM) from breast cell lines (M1, MDA-MB-21 or MCF7). Expression was normalized to the parallel time control of normal medium treatment. The results are expressed as the mean ± s.d, n = 3. Student's t test, *$P < 0.05$, ***$P \leq 0.001$. **B**, *TGFB1*, *TGFB2*, *TGFB3*, *TNFA*, *IL1B* mRNA levels in 52 breast cancer cell

lines. The expression levels were categorized to 4 groups: Background, Low, Intermediated, High. **C**, *TGFB1/2/3*, *TNFA*, *IL1B* expression in primary breast cancer samples. The expression level was categorized to 4 groups: Background, Low, Intermediated, High. **D**, TGFβ3 (5 ng/ml), or TNFα (10 ng/ml), or IL1β (10 ng/ml) induce *GREM1* expression in 19TT cancer-associated fibroblasts (CAFs). Expression was normalized to the parallel time control of buffer treatment. The results are expressed as the mean ± s.d., n = 3. Student's t test, *$P < 0.05$, **$P \leq 0.01$, ***$P \leq 0.001$. **E**, Measurements of TGFβ activity in CM from breast cancer cell lines using a CAGA luciferase (LUC) reporter assay in HEK293T cells as read out. TGFβ neutralizing antibody (10 ng/ml) was added to demonstrate that luciferase activity in CM is due to TGFβ activation and not activins or nodal. Recombinant TGFβ was added to control for functionality of the assay. The value are normalized to β-galactosidase(βGal) activity. The results are expressed as the mean ± s.d, n = 3. Student's t test, ***$P \leq 0.001$. **F**, The induction of *GREM1* expression in 19TT CAFs by CM from MCF7 and MDA-MB-21 is blocked by TGFβ neutralizing antibody. The results are expressed as the mean ± s.d, n = 3. Student's t test, **$P \leq 0.01$.

factors secreted by cancer or inflammatory cells. We first collected CM from M1 immortalized normal breast cells, and breast cancer cell lines MCF7 and MDA-MB-231. Treatment of 19TT CAFs (Figure 2A) or W21 MSCs (Figure S2A) with MDA-MB-231 or MCF7 cells CM resulted in a significant increase in *GREM1* mRNA levels. There was no effect of M1 CM on *GREM1* expression. To explore the factors that are responsible for inducing *GREM1* expression in CAFs, we analyzed by data mining the expression of *TGFB1/2/3* and inflammatory cytokines in breast cancer cell lines as well as in breast cancer tissues. We found that *TGFB1/2/3* are highly expressed in both breast cancer cell lines and tissues. Inflammatory cytokines, including *IL1B* and *TNFA*, were expressed in breast cancer tissues but only at very low levels in breast cancer cell lines (Figure 2B and C). *IL1B* and *TNFA* expression in breast cancer tissues is thus likely caused by the stromal cells present in breast cancer tissue samples. Challenging 19TT CAFs (Figure 2D) or W21 MSCs (Figure S2B) with TGFβ3, TNFα, and IL1β promoted *GREM1* mRNA expression. Next we analyzed whether TGFβ is secreted by cancer cells. MDA-MB-231 and MCF7, but not M1, were found to express active TGFβ (Figure 2E). Importantly, the GREM1 expression-inducing activity of MDA-MB-231 or MCF7 cells could be blocked by a TGFβ neutralizing antibody (Figure 2F). Taken together, TGFβ secreted by cancer cells is the main determinant for inducing *GREM1* expression by CAFs. Within the tumor-stroma niche, inflammatory cells secreting cytokines may also contribute to *GREM1* expression by CAFs.

81

Grem1 increases mammosphere formation

BMPs are reported to be inhibitors of cell stemness, suggesting that secreted Grem1 might oppositely affect stem traits [9, 22, 46]. First, we confirmed that *BMPs* and *BMP receptors* are indeed expressed in breast cancer cell lines (Figure 1B, Figure S3A and B). Then, mammosphere
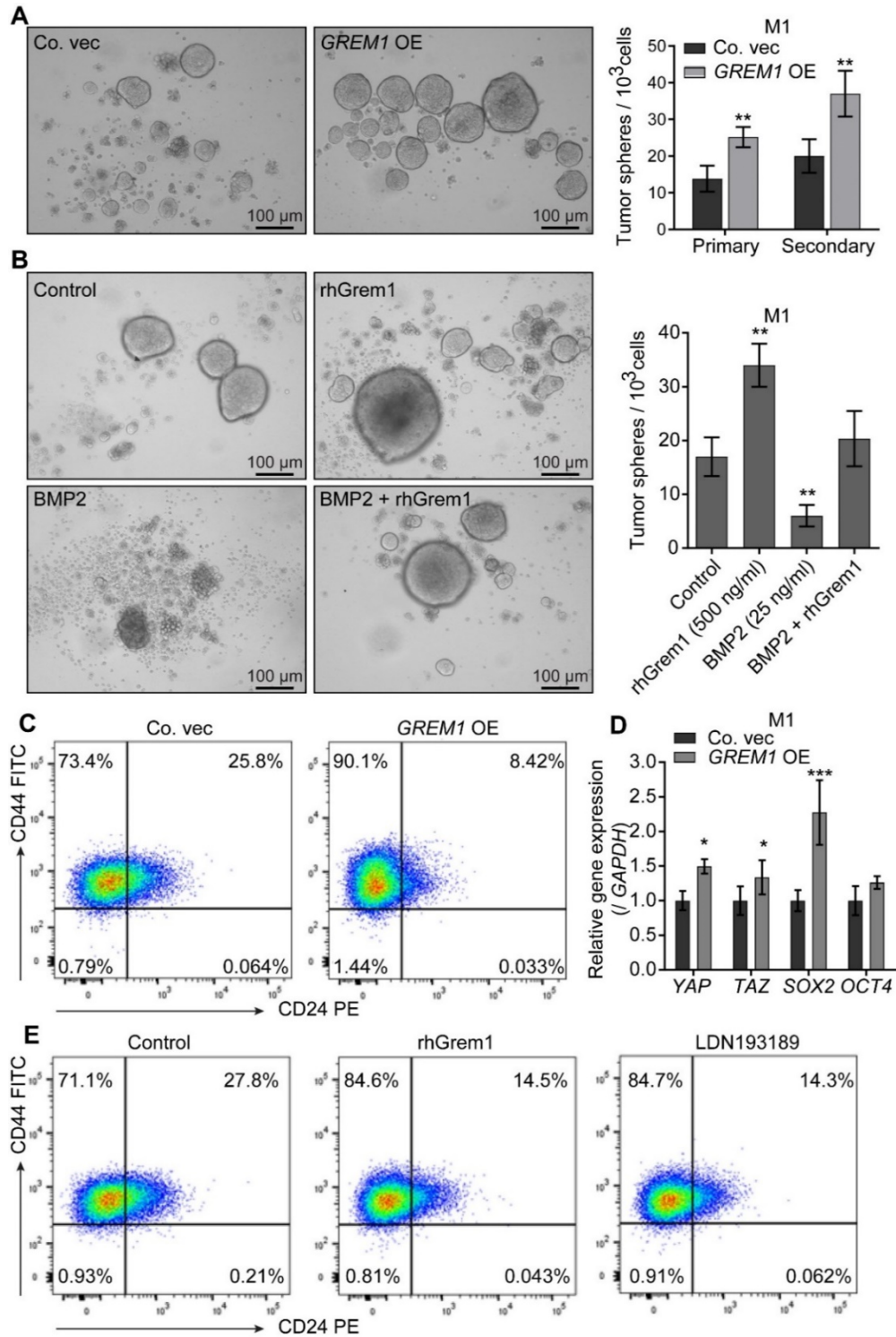
Figure 3. Grem1 maintains stemness in M1 cells. A, *GREM1* overexpression (OE) induces more mammosphere formation in M1 cells. Left, representative images of mammospheres at 7 days. Right, number of spheres formed per 1000 cells plated. The primary spheres were disintegrated and replated further. Secondary spheres formed were counted. The results are expressed as the mean ± s.d., n = 3. Student's t test, **$P \leq 0.01$. **B**, Pro-mammosphere formation ability of recombinant human Grem1 (rhGrem1) protein (500 ng/ml) can be neutralized by BMP2 (50 ng/ml). Left, representative images of spheres at 7 days; Right, number of spheres formed per 1000 cells plated. The results are expressed as the mean ± s.d., n = 3. Student's t test, **$P \leq 0.01$. **C**, Flow cytometry analysis shows that *GREM1* OE in M1 cells increases the stem population (CD44$^{+/high}$ CD24$^{-/low}$). **D**, *GREM1* OE in M1 cells upregulates stem cell transcription factors. *GAPDH* was used as an internal control. The results are expressed as the mean ± s.d., n = 3. Student's t test, *$P < 0.05$, ***$P \leq 0.001$. **E**, Flow cytometry analysis showing that 2 days of treatment with rhGrem1 (500 ng/ml) or the BMP type I receptor inhibitor LDN193198 (120 nM) also leads to an increase in the CD44$^{+/high}$ CD24$^{-/low}$ population.

formation assay was performed to assess the effect of Grem1 on mammary stem cell activity *in vitro*. *GREM1*-overexpressing M1 cells exhibited two-fold more sphere formation compared to control cells in each of two subsequent passages (Figure 3A). The administration of exogenous rhGrem1 showed a similar effect on mammosphere formation of M1 cells, whereas the administration of exogenous BMP2 mitigated sphere formation ability. The latter could be reversed by the concurrent administration of rhGrem1 (Figure 3B). The surface expression of CD44$^{+/high}$ CD24$^{-/low}$ cells has been considered a stem population marker of breast cancers or cell lines [46]. Flow cytometry analysis demonstrated a significant increase in the CD44$^{+/high}$ CD24$^{-/low}$ cell subpopulation in *GREM1*-overexpressing M1 cells compared to the control (Figure 3C). qRT-PCR revealed that *GREM1* OE (Figure 3D) or rhGrem1 (Figure S3C) increased the expression of transcriptional regulators *YAP*, *TAZ*, *SOX2*, and *OCT4*, which have been implicated in maintaining breast cancer stemness. Moreover, M1 cells treated with rhGrem1 or the BMP type I receptor inhibitor LDN193189 [47] also displayed more CD44$^{+/high}$ CD24$^{-/low}$ cells than non-treated control cells (Figure 3E). These results suggest that Grem1 enhances the mammosphere formation of M1 cells by repressing BMP signaling.

Grem1 promotes breast cancer cell invasion

To further characterize the role of Grem1 in breast cancer, we stably expressed Grem1 in the breast cancer cell lines M2 and MDA-MB-231 with a lentiviral vector. In a way these transfected
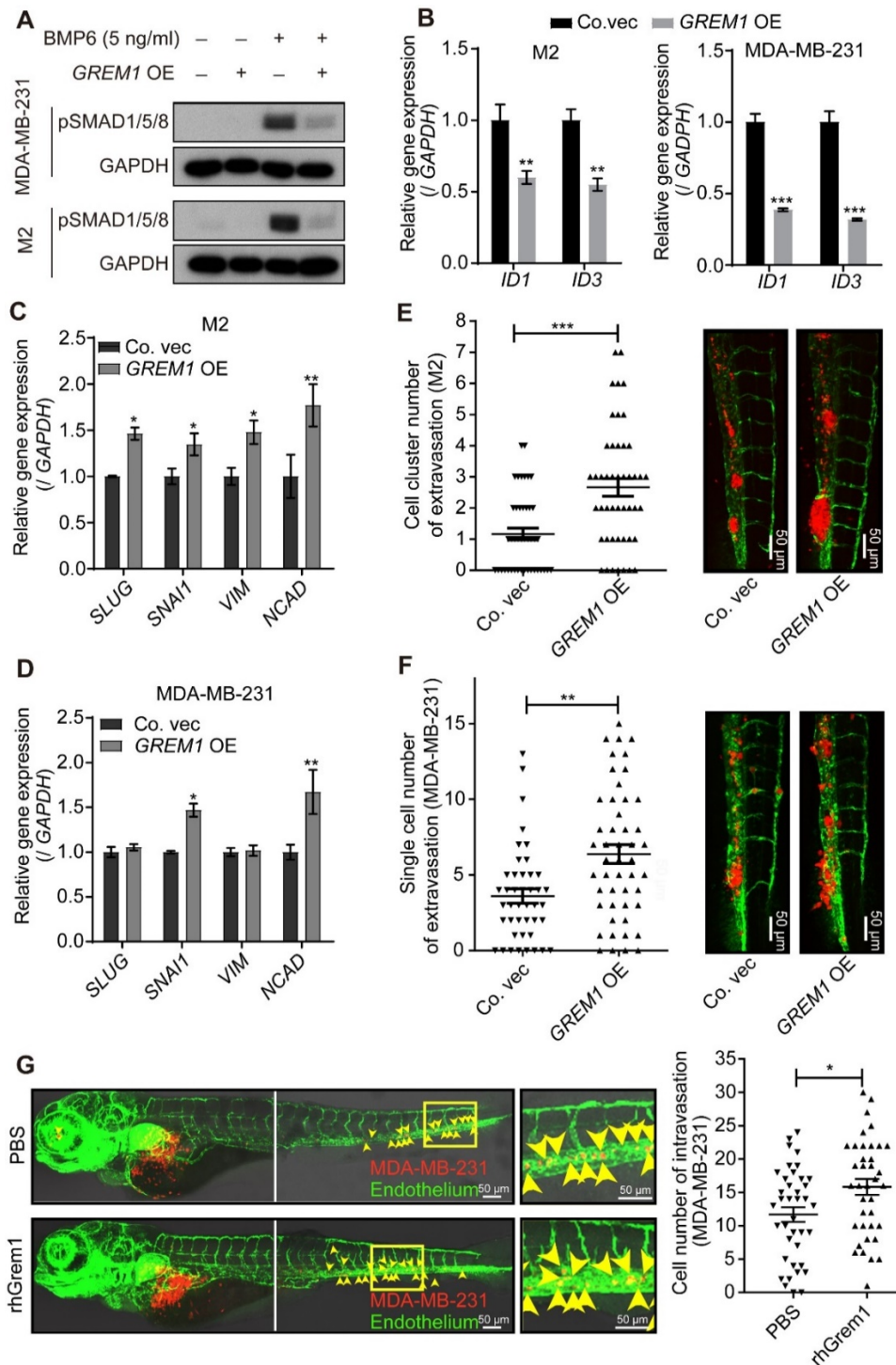
Figure 4. Ectopic expression of *GREM1* promotes cancer cell invasion in a zebrafish model. A, **B**, *GREM1* overexpression (OE) inhibits BMP-induced SMAD1/5/8 phosphorylation (pSMAD1/5/8, **A**) and the BMP target genes *ID1* and *ID3* (**B**) in MDA-MB-231 and M2 cell lines. *GAPDH* was used as an internal control. The results are expressed as the mean ± s.d., n = 3. Student's t test, **$P \leq 0.01$. **C**, **D**, *GREM1* OE upregulates the expression of EMT transcription factors and markers in M2 (**C**) and MDA-

MB-231 (**D**) cells. *GAPDH* was used as an internal control. The results are expressed as the mean $\pm$ s.d., n = 3. Student's t test, **$P \leq 0.01$. **E**, **F**, *GREM1* OE induces more clusters formation in M2 cells (**E**) and promotes the invasion of MDA-MB-231 cells (**F**) in zebrafish. Left, quantification of the number of extravasated cells/clusters at 5 days post injection (dpi). Right, representative images; Green, vasculature of zebrafish; Red, mCherry-labeled cells. The results are expressed as the mean $\pm$ s.e.m., n=2. Student's t test, **$P \leq 0.01$, ***$P \leq 0.001$. **G**, Perivitelline space injection of MDA-MB-231 cells supplemented with rhGrem1 (1 µg/ml) increases cell intravasation in zebrafish. Left, representative images. Green, vasculature of zebrafish; Red, mCherry-labeled cells. Right, quantification of the number of intravasated cells in each embryonic body at 3 days post injection (dpi). The results are expressed as the mean $\pm$ s.e.m., n=2. Student's t test, *$P < 0.05$.

cell lines are somewhat reminiscent to the few breast cancer cell lines that express *GREM1*. In these *GREM1*-overexpressing cell lines, BMP-induced SMAD1/5/8 phosphorylation (Figure 4A) and expression of BMP target genes ID1 and 3 (Figure 4B) were clearly inhibited. Notably, the mRNA levels of the mesenchymal markers *SLUG*, *SNAI1*, *VIM*, and *NCAD* were increased by ectopic *GREM1* expression (Figure 4C and D) or exogenous rhGrem1 treatment (Figure S4B), suggesting that Grem1 induces a slightly more mesenchymal phenotype in these breast cancer cells. To test whether exposure to Grem1 also results in more invasive behavior, we introduced these cells into the blood circulation of embryonic zebrafish via DoC injection and examined extravasation 5 days post injection (dpi) in the avascular tail fin area. Compared to the vector control, the *GREM1* overexpression group showed a higher number of extravasated M2 cell clusters (Figure 4E) or MDA-MB-231 single cells (Figure 4F). The BMP/SMAD signaling could be inhibited by exogenous administration of rhGrem1 (Figure S4B). Next, we injected MDA-MB-231 cells suspended in PBS supplemented with or without rhGrem1 into the perivitelline space of embryonic zebrafish and examined the level of cells in circulation at 3 dpi. Exogeneous rhGrem1 increased cellular intravasation significantly, as more cells were found in the head and tail regions of zebrafish embryos (Figure 4G).

Grem1 promotes fibroblast activation

Grem1 is associated with fibrosis [17-19]. To explore the role of Grem1 in fibroblast activation, we first compared *GREM1* mRNA expression levels in foreskin fibroblasts, 19TT breast cancer CAFs, and HM, W18 and W21 human mesenchymal stem cells (MSCs). M2, MCF7 and MDA-MB-231 cancer cells served as negative control. MSCs, which are considered fibroblast

85

precursors and can differentiate into fibroblasts [2], showed the lowest expression of *GREM1*; *GREM1* expression in the foreskin fibroblasts, which represent normal fibroblasts, was significantly higher than that in MSCs, and 19TT CAFs showed the highest levels (Figure 5A), indicating that *GREM1* expression increases during different stages of fibroblast activation. We next knocked down *GREM1* in 19TT CAFs. As shown in Figure 5B, two shRNAs-mediated *GREM1* knockdown increased the mRNA expression of both *ID1* and *ID3* and decreased the expression of TGFβ signaling components and their target genes (*Plasminogen activator inhibitor (PAI-1)*), fibroblast activation markers and *matrix metalloproteinases* (*MMPs*). *GREM1* knockdown in 19TT CAFs also led to decreased protein levels of FN1, S100A4, Collagen I, FAP, and αSMA (Figure 5C). This result suggests that Grem1 is a pivotal factor in fibroblast activation.

To examine whether Grem1 affects cytoskeletal changes, we stained the cells with fluorescein-conjugated phalloidin to visualize filamentous (F)-actin. Indeed, *GREM1* knockdown in 19TT CAFs resulted in less prominent stress fibers and less organized bundles in the cytoplasm (Figure 5D). More significantly, the ability of 19TT CAFs to contract collagen gels (a 3D model widely used for evaluating fibroblast-mediated matrix remodeling capacity) decreased significantly with *GREM1* knockdown (Figure 5E). Moreover, *GREM1* overexpression in W21 MSCs (Figure S5A) induced intensive myofibroblast-like characteristics (Figures S5B-E). Consistent with this result, W21 MSCs treated with rhGrem1 or the selective BMP receptor kinase inhibitor LDN193189 exhibited an upregulation of genes which were inhibited by *GREM1* knockdown in 19TT CAFs (Figure S2F). Overall, these observations imply that Grem1 is closely associated with the fibrogenic phenotype of breast CAFs.

Figure 5. *GREM1* knockdown in 19TT breast cancer-associated fibroblasts (CAFs) attenuates fibrotic characteristics. A, qRT-PCR comparison of relative *GREM1* expression in M2, MCF7, MDA-MB-231,HM, W18, and W21 fetal mesenchymal stem cells (MSCs), foreskin fibroblasts and 19TT CAFs. *GAPDH* was used as an internal control. The results are expressed as the mean ± s.d., n=3. Student's t test, **$P \leq 0.01$, ***$P \leq 0.001$. **B**, qRT-PCR analysis of selected genes, BMP targets, TGFβ pathway constituents/targets, fibroblast activation markers, and matrix metalloproteinases in 19TT CAFs with/without shRNA-mediated *GREM1* knockdown. *GAPDH* was used as an internal control. The results are expressed as the mean ± s.d., n = 3. Student's t test, *$P < 0.05$, **$P \leq 0.01$, ***$P \leq 0.001$. **C**, Western blot analysis to detect changes in indicated proteins after *GREM1* knockdown in 19TT CAFs. **D**,
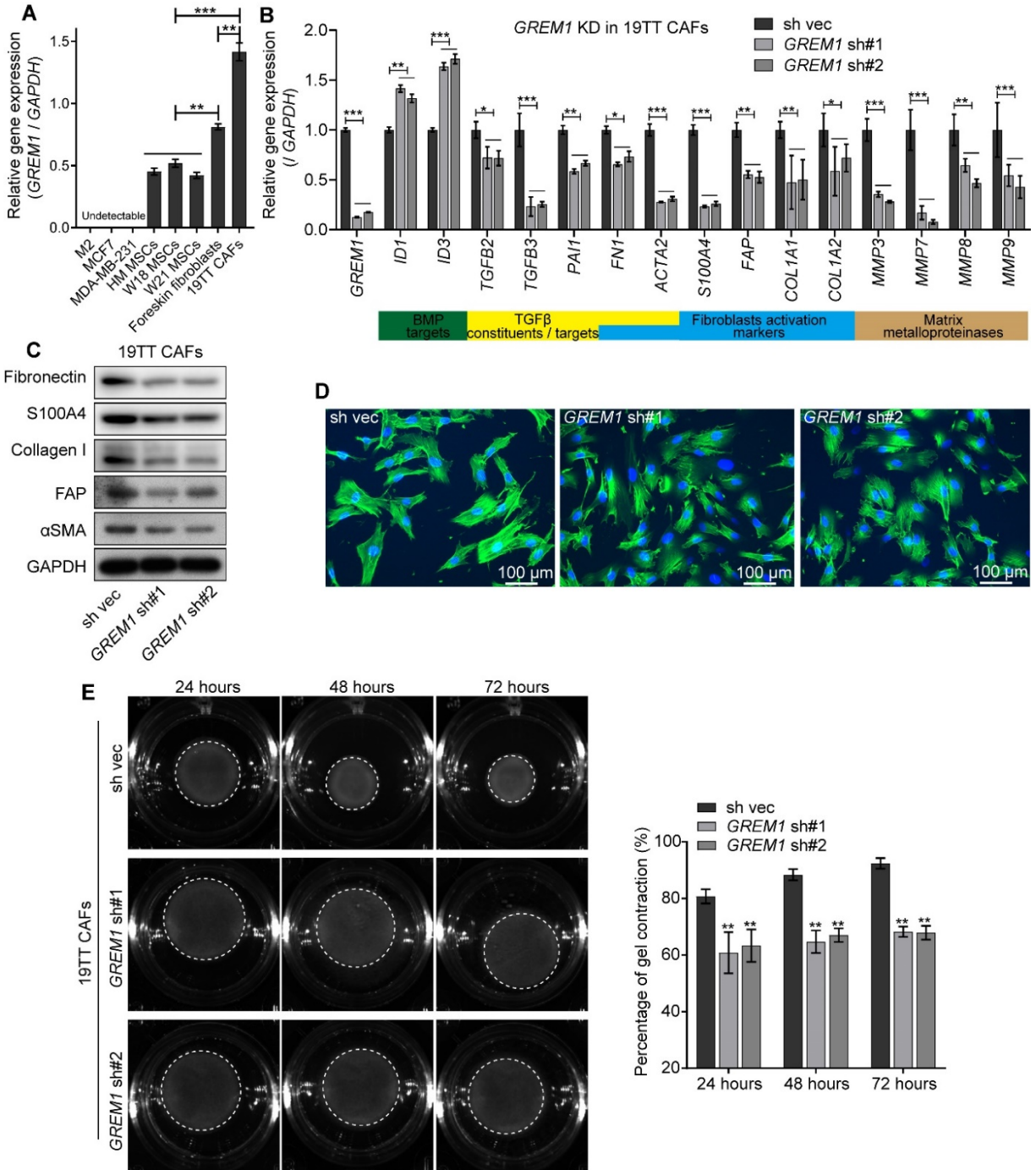
19TT CAFs with/without *GREM1* knockdown were stained with fluorescein-phalloidin (green) to visualize F-actin. DAPI was used for nuclear staining (blue). **E**, Collagen gel contraction assay. 19TT CAFs with/without *GREM1* knockdown were embedded in collagen gels. After 24, 48, and 72 h, the area of each gel (white dash circle) was imaged and quantified. Left, Representative images of contracted gels. Right, percentage of gel contraction. Quantification is shown in the Methods. The results are expressed as the mean ± s.d., n = 3. Student's t test, **$P \leq 0.01$.

Fibroblast-derived Grem1 promotes breast cancer cell invasion in a 3D spheroid model

Previous studies have indicated that CAFs are propellants of cancer cell invasion [1, 2]. Prompted by the profibrotic role of Grem1, we further explored the roles of Grem1 in fibroblast-mediated cancer cell invasion using a 3D spheroid model. As illustrated in Figure S6A, spheroids
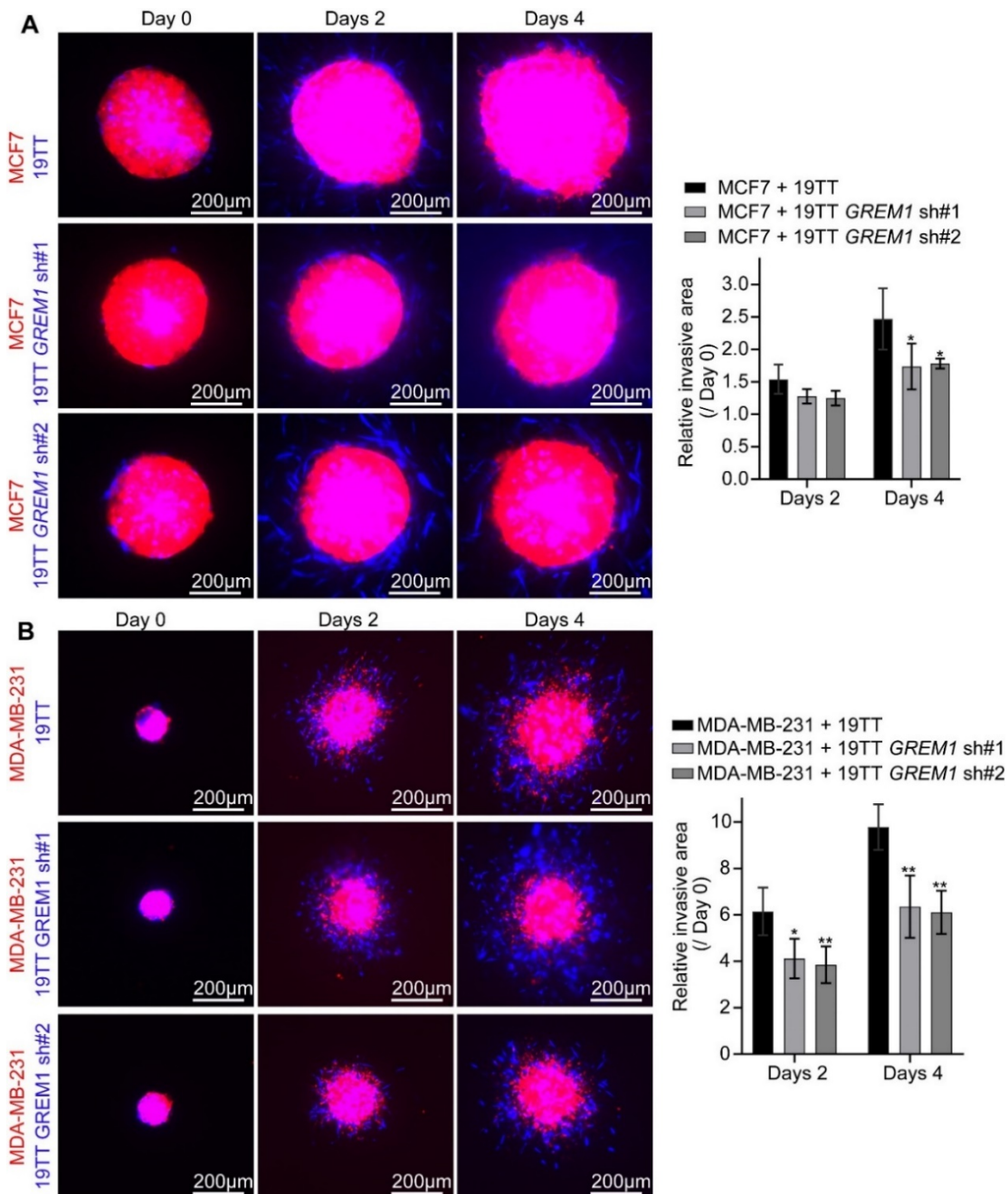
Figure 6. *GREM1* knockdown in 19TT breast cancer-associated fibroblasts (CAFs) impairs breast cancer cells invasion in a 3D spheroid invasion model. A, **B**, Collagen invasion assay of co-culture spheroids. Eight spheroids per indicated group were embedded into collagen. Left, representative images

of 3D spheroid invasion at days 0, 2, and 4. Red, MCF7 (**A**) or MDA-MB-231 (**B**) cells; Blue, 19TT cells with/without *GREM1* knockdown. Right, relative invasion area was quantified as the area difference at days 2 and 4 relative to that at day 0. The results are expressed as the as the mean $\pm$ s.d., n = 8. Student's t test, *$P < 0.05$, **$P \leq 0.01$.

were produced from hanging drop co-cultures of mCherry-labeled breast cancer cells, MCF7 or MDA-MB-231 cells, and AmCyan-labeled 19TT CAFs. CAFs with or without *GREM1* knockdown were mixed with these breast cancer cells at a 1:1 ratio. the various resulting spheroids were embedded in collagen gel. As shown in Figure S6B, the monocultured MCF7 spheroid showed a collective cells invasion phenotype in collagen, and in the presence of 19TT cells, the increased invasion of CAFs was measured at days 4. However, upon *GREM1* depletion in the 19TT CAFs, the coculture spheroids showed strongly reduced invasion (Figure 6A). Likewise, *GREM1* knockdown in the CAFs reduced the invasion of MDA-MB-231 cells in MDA-MB-231 and 19TT co-culture spheroids at days 2 and 4 (Figure 6B).

Fibroblast-derived Grem1 promotes breast cancer cell intravasation

Next, we examined the role of fibroblast-expressed Grem1 in breast cancer cell invasion *in vivo*. We injected mCherry-labeled MDA-MB-231 cells into the perivitelline space of zebrafish in the absence or presence of either AmCyan-labeled W21 MSCs, foreskin fibroblasts, or 19TT CAFs. As depicted in Figure 7A, intravasation of the MDA-MB-231 cells was significantly increased when co-implanted with W21, validating a previous study in which MSCs promoted cancer metastasis [48]. Importantly, this intravasation was much more enhanced by the foreskin fibroblasts and even more so by the 19TT CAFs, suggesting a correlation with their *GREM1* expression level. Indeed, the ectopic expression of *GREM1* in W21 cells resulted in enhanced MDA-MB-231 cells intravasation upon co-injection (Figure S7). Consistent with this result, *GREM1* knockdown mitigated the promotion role of 19TT CAFs on MDA-MB-231 cells intravasation (Figure 7B).

Discussion

Our work has uncovered a strong association between high *GREM1* expression in breast tumor biopsies and a poor prognosis. We provide mechanistic insights into GREM1's key role in facilitating breast cancer progression using *in vitro* and *in vivo* studies. Grem1 is highly expressed by CAFs at the invasion front; its expression can be promoted by factors, such as
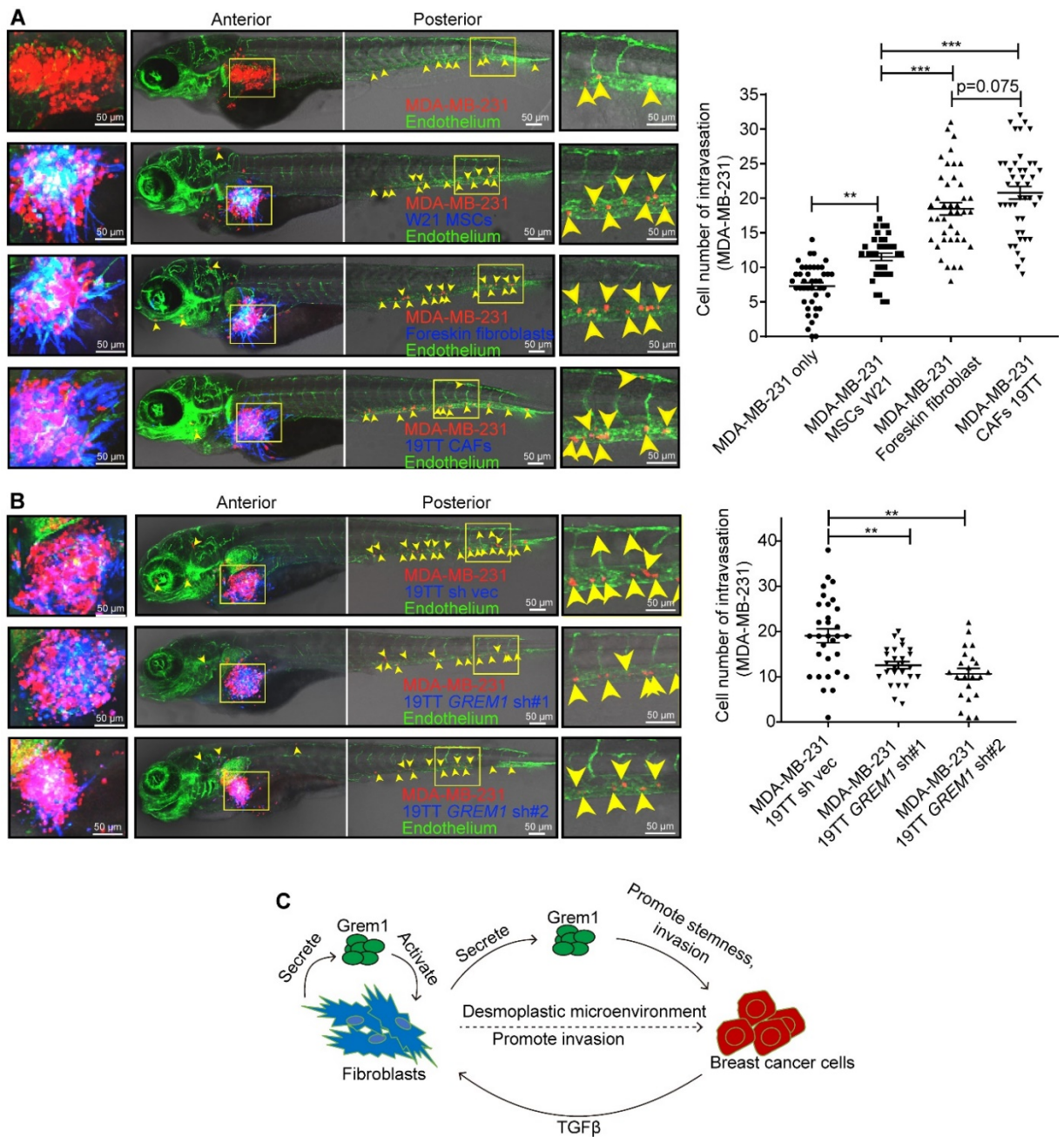
Figure 7. *GREM1* knockdown attenuates the ability of 19TT breast cancer-associated fibroblasts (CAFs) to promote breast cancer cell intravasation in a zebrafish co-injection model. A, Perivitelline space single injection of MDA-MB-231 cells or co-injection of MDA-MB-231 cells and W21 mesenchymal stem cells (MSCs), foreskin fibroblasts or 19TT CAFs, as indicated. The panel shows representative images. Green, endothelium of zebrafish; red, mCherry-labeled MDA-MB-231; Blue, converted from AmCyan-labeled MSCs or fibroblasts. Yellow arrowheads point to single intravasated cells in the head and tail regions of zebrafish. Left, cell migration in the perivitelline space; Middle, image

of a zebrafish embryo body; Right, visualization of intravasated cells in the posterior of the embryo. The graph shows the quantification of the number of intravasated cells in each embryonic body at 3 days post injection (dpi). The results are expressed as the mean ± s.e.m., n=2. Student's t test, **$P \leq 0.01$, ***$P \leq 0.001$. **B**, Perivitelline space co-injection of MDA-MB-231 cells and 19TT CAFs with/without *GREM1* knockdown. The panel and graph description are the same as described in (**A**). The results are expressed as the mean ± s.e.m., n=2. Student's t test, **$P \leq 0.01$. **C**, Schematic of the working model of Grem1 function in breast cancer progression. Grem1 expression in fibroblasts is induced by factors (such as TGFβ from breast cancer cells or maybe other stromal cells (that produce inflammatory cytokines). Grem1 could activate fibroblasts into CAFs. CAFs might present a desmoplastic microenvironment, thereby promote cancer cell invasion. Grem1 itself could promote the stemness, and invasion of breast cancer cells.

TGFβ released by breast cancer cells and inflammatory cytokines. Grem1 mediates the fibrogenic activation of CAFs in an autocrine manner. Grem1 has a direct effect on cancer cell invasion and stemmness, evidenced by the fact that it promoted a slightly more mesenchymal/stemness phenotype in breast cancer cells. It could also contribute indirectly to this process via its potent effects on fibroblast activation. In this way, Grem1 promotes the formation of a microenvironment conducive to breast cancer cell invasion. Thus, Grem1 is a key determinant of the mutual interplay between breast cancer cells and CAFs (Figure 7C).

Although we found an association between Grem1 and poor breast cancer prognosis, the prognostic significance of Grem1 in different cancer types is not consistent. For example, Grem1 expression correlates with progression-free survival in pancreatic neuroendocrine tumors [49] and colorectal cancer [50], but it is an indicator of poor progression-free survival in cervical cancer [51]. Grem1 may have different roles in different tumor types, but this may be dependent on the experimental setup, the analysis of expression in complete tumors versus stromal expression specifically, and/or the determining the levels of RNA versus protein. For instance, when testing commercial antibodies on tissue sections, including sections of *GREM1*-deficient animals, we found that the detected signals may not have been specific for Grem1 (data not shown). To avoid these putatively non-specific measurements, we determined *GREM1* mRNA levels by *in situ* hybridization.

The mRNA detection method revealed that *GREM1* was exclusively expressed by CAFs. Our findings are supported by our data mining of publicly available data sets. We analyzed breast cancer dataset *GSE14548* generated by Ma and colleagues [28], which separated epithelial

and stroma tissues, and in this dataset *GREM1* was found mainly expressed in the (invasive) breast cancer stroma, and there was no *GREM1* expression observed in normal epithelium and stroma (Figures S8a). In addition, we mined a colon cancer dataset *GSE39396* in which epithelial cells, leukocytes, fibroblasts and endothelial cells were separately isolated by FACs and thereafter profiled. Consistent with our results, only fibroblasts were found to express *GREM1* (Figures S8b).

We found that *GREM1* expression in CAFs is particularly high in close vicinity of cancer cells. This is consistent with previous reports in which Grem1 was found to be highly expressed in CAFs in the microenvironment of basal cell carcinoma (and other tumors) compared to normal tissue counterparts [23], and a study of colorectal cancer, in which Grem1 was found to be expressed at the invasion fronts in CAFs, and to mediate the loss of cancer cell differentiation [3]. We identified TGFβ secreted by cancer cells as a strong driver of *GREM1* expression by CAFs. Moreover, clinical breast cancer samples were also found to highly express *TGFB1/2/3* suggesting that these findings are of clinical relevance. Such invasion fronts are rich in inflammatory cells [52]. Consistent with this result, we found that inflammatory cytokines IL1β and TNFβ induced *GREM1* expression in CAFs. Moreover, *GREM1* expression correlated with mesenchymal marker expression in tumor samples. The latter observation indicates that Grem1 at the invasion front may contribute to the desmoplastic phenotype (Figure 7C).

We observed a striking activation of fibrogenesis in fibroblasts and in CAFs by Grem1. Depletion or ectopic expression of Grem1 in CAFs demonstrated that Grem1 expression is positively linked to expression of TGFβ ligands and target genes, mesenchymal markers, extracellular matrix proteins and matrix metalloproteinase (MMP) remodeling factors at the mRNA level, as well as with Fibronectin, S100A4, Collagen I, FAP, and αSMA at the protein level. In addition, Grem1 promoted actin stress fiber formation and collagen gel contraction. These expression patterns are characteristic of a fibrogenic response and fibroblast activation. The Grem1-induced responses may be mediated by TGFβ pathway activation; TGFβ is a strong inducer of fibrogenesis and an activator of fibroblasts [53]. With TGFβ being a strong inducer of Grem1 and *vice versa,* it may act in a feed forward loop.

Multiple studies have shown that CAFs create a microenvironment suitable for cancer cell invasion [1, 2], which we further demonstrated in this study *in vivo* by co-injection of breast cancer cells with fibroblasts/CAFs into the zebrafish perivitelline space. Thus, the profibrogenic

ability of Grem1 could contribute to its role in promoting cancer cell invasion mediated by activated fibroblasts and CAFs. 3D coculture of breast cancer cells with CAFs in collagen demonstrated that Grem1 is critical for invasion. In accordance with these results, Grem1 strongly promoted intravasation in a zebrafish co-injection xenograft model. Moreover, by injecting ectopic Grem1-producing M2 and MDA-MB-231 cells into the DoC of zebrafish embryos, we found that Grem1 strongly promoted the extravasation of cancer cells. These results may explain the clinical association between Grem1 expression in tumors and a poor prognosis of MFS.

Mechanistically, Grem1 exerts its effects by antagonizing selective BMPs [11]. Consistent with this notion, we found that BMP-induced SMAD1/5 phosphorylation is inhibited in breast cancer cells and in CAFs. In addition, depletion of endogenous Grem1 in CAFs upregulates BMP/SMAD-dependent *ID1*/*ID3* expression whilst addition of rhGrem1 has the opposite effect. Moreover, treatment with a selective BMP receptor kinase inhibitor mimicked the effect of exogenous Grem1 protein by promoting mammosphere formation and fibrogenic marker expression. However, our results do not exclude the possibility that Grem1 also can act via BMP-independent pathways [24]. For example, induction of TGFβ expression by Grem1 may occur independently of BMP antagonism. Grem1 was found to promote cell viability, migration and invasion in glioma [54] and the invasive phenotype of mesothelioma [55] by activating TGFβ/SMAD signaling. Moreover, Grem1 may promote breast tumorigenesis by acting on signaling pathways distinct from TGFβ family signaling; in renal tubular cells, Grem1 has been reported to signal via the vascular endothelial growth factor receptor 2 (VEGFR2) pathway [21] to promote angiogenesis [56] and to mediate inflammation and the infiltration of immune-inflammatory cells [57]. Furthermore, Grem1 may act directly or indirectly by sequestering BMP on endothelial cells and immune cells and thereby promote tumorigenesis. Irrespective of the precise mechanisms, our results demonstrate potent pro-tumorigenic effects of Grem1 on cancer cells and CAFs *in vitro* in mono- and in co-culture, as well as a key *in vivo* role for Grem1 in stimulating extravasation and for Grem1-producing CAFs in mediating the intravasation of breast cancer cells. These two processes, extravasation and intravasation, are key steps in the dissemination and distant colonization of primary cancer cells.

Our results identified Grem1 as a driving force of breast cancer progression by affecting the behavior of both cancer cells and neighboring CAFs. Antibodies that neutralize Grem1's

function in the Grem1-BMP interaction have been described which may be beneficial not only for the treatment of pulmonary arterial hypertension [58] but also for breast cancer (by inhibiting breast cancer progression). In addition, BMP agonists that are engineered to prevent interactions with Grem1, as has been performed for Noggin [59], or BMP-mimetic small molecule drugs [60, 61], could be beneficial in the treatment of breast cancer patients with high Grem1 expression.

Acknowledgements

Funding

Availability of data and materials

All remaining data and materials are available from the authors upon reasonable request

Authors' contributions

Conceptualization PtD, JWMM, JR; Methodology: JR; Acquisition of data: PtD, JWMM, JR; Writing, review, and/or revision of the manuscript: JR, PtD, HvD; Administrative, technical, or material support: PtD, JWMM, JR, MS, DCFS, JI, HJZ; Study supervision: PtD.

Ethics approval and consent to participate

All research using zebrafish, including housing and experiments, was carried out according to the international guidelines and was approved by the local Institutional Committee for Animal Welfare (*Dier Ethische Commissie* (DEC)) of the LUMC.

References

1. Madar S, Goldstein I, Rotter V. 'Cancer associated fibroblasts'–more than meets the eye. Trends Mol Med 2013, 19(8):447-53.

2. Kalluri R. The biology and function of fibroblasts in cancer. Nat Rev Cancer 2016, 16(9):582-8.

3. Karagiannis GS, Poutahidis T, Erdman SE, *et al*. Cancer-associated fibroblasts drive the progression of metastasis through both paracrine and mechanical pressure on cancer tissue. Mol Cancer Res 2012, 10(11):1403-18.

4. Katagiri T, Watabe T. Bone morphogenetic proteins. Cold Spring Harb Perspect Biol 2016, 8(6):a021899.

5. Ren J, ten Dijke P. Bone morphogenetic proteins in the initiation and progression of breast cancer. Bone Morphogenetic Proteins: Systems Biology Regulators, Springer 2017, p.409-33.

6. Brazil DP, Church RH, Surae S, *et al*. BMP signalling: agony and antagony in the family. Trends Cell Biol 2015, 25(5):249-64.

7. Tarragona M, Pavlovic M, Arnal-Estapé A, *et al*. Identification of NOG as a specific breast cancer bone metastasis-supporting gene. J Biol Chem 2012, 287(25):21346-55.

8. Mock K, Preca B, Brummer T, *et al*. The EMT-activator ZEB1 induces bone metastasis associated genes including BMP-inhibitors. Oncotarget 2015, 6(16):14399-412.

9. Gao H, Chakraborty G, Lee-Lim AP, *et al*. The BMP inhibitor Coco reactivates breast cancer cells at lung metastatic sites. Cell 2012, 150(4):764-79.

10. Nolan K, Thompson TB. The DAN family: Modulators of TGF-β signaling and beyond. Protein Science 2014, 23(8):999-1012.

11. Church RH, Krishnakumar A, Urbanek A, *et al*. Gremlin1 preferentially binds to bone morphogenetic protein-2 (BMP-2) and BMP-4 over BMP-7. Biochem J 2015, 466(1):55-68.

12. Khokha MK, Hsu D, Brunet LJ, *et al*. Gremlin is the BMP antagonist required for maintenance of Shh and Fgf signals during limb patterning. Nat Genet 2003, 34(3):303-7.

13. Michos O, Panman L, Vintersten K, *et al*. Gremlin-mediated BMP antagonism induces the epithelial-mesenchymal feedback signaling controlling metanephric kidney and limb organogenesis. Development 2004, 131(14):3401-10.

14. Mangold E, Ludwig KU, Birnbaum S, *et al*. Genome-wide association study identifies two susceptibility loci for nonsyndromic cleft lip with or without cleft palate. Nat Genet 2010, 42(1):24-6.

15. Tardif G, Pelletier JP, Boileau C, *et al*. The BMP antagonists follistatin and gremlin in normal and early osteoarthritic cartilage: an immunohistochemical study. Osteoarthritis Cartilage 2009, 17(2):263-70.

16. Gazzerro E, Pereira RC, Jorgetti V, *et al*. Skeletal overexpression of gremlin impairs bone formation and causes osteopenia. Endocrinology 2005, 146(2):655-65.

3

17. Boers W, Aarrass S, Linthorst C, *et al*. Transcriptional profiling reveals novel markers of liver fibrogenesis: gremlin and insulin-like growth factor-binding proteins. J Biol Chem 2006, 281(24):16289-95.

18. Koli K, Myllärniemi M, Vuorinen K, S *et al*. Bone morphogenetic protein-4 inhibitor gremlin is overexpressed in idiopathic pulmonary fibrosis. Am J Pathol 2006, 169(1):61-71.

19. Walsh DW, Roxburgh SA, McGettigan P, *et al*. Co-regulation of Gremlin and Notch signalling in diabetic nephropathy Biochim Biophys Acta 2008, 1782(1):10-21.

20. Corsini M, Moroni E, Ravelli C, *et al*. Cyclic adenosine monophosphate-response element-binding protein mediates the proangiogenic or proinflammatory activity of gremlin. Arterioscler Thromb Vasc Biol 2014, 34(1):136-45.

21. Mitola S, Ravelli C, Moroni E, *et al*. Gremlin is a novel agonist of the major proangiogenic receptor VEGFR2. Blood 2010, 116(18):3677-80.

22. Yan K, Wu Q, Yan DH, *et al*. Glioma cancer stem cells secrete Gremlin1 to promote their maintenance within the tumor hierarchy. . Genes Dev 2014, 28(10):1085-100.

23. Sneddon JB, Zhen HH, Montgomery K, v *et al*. Bone morphogenetic protein antagonist gremlin 1 is widely expressed by cancer-associated stromal cells and can promote tumor cell proliferation. Proc Natl Acad Sci U S A 2006, 103(40):14842-7.

24. Kim M, Yoon S, Lee S, *et al*. Gremlin-1 induces BMP-independent tumor cell proliferation, migration, and invasion. PLoS One 2012, 7(4):e35100.

25. Jaeger E, Leedham S, Lewis A, *et al*. Hereditary mixed polyposis syndrome is caused by a 40-kb upstream duplication that leads to increased and ectopic expression of the BMP antagonist GREM1. Nat Genet 2012, 44(6):699-703.

26. Davis H, Irshad S, Bansal M, *et al*. Aberrant epithelial GREM1 expression initiates colonic tumorigenesis from cells outside the stem cell niche. Nat Med 2015, 21(1):62-70.

27. Karagiannis GS, Berk A, Dimitromanolakis A, *et al*. Enrichment map profiling of the cancer invasion front suggests regulation of colorectal cancer progression by the bone morphogenetic protein antagonist, gremlin-1. Mol Oncol 2013, 7(4):826-39.

28. Ma XJ, Dahiya S, Richardson E, E *et al*. Gene expression profiling of the tumor microenvironment during breast cancer progression. Breast Cancer Res 2009, 11(1):R7.

29. Kim HS, Shin MS, Cheon MS, *et al*. GREM1 is expressed in the cancer-associated myofibroblasts of basal cell carcinomas. PLoS One 2017, 12(3):e0174565.

30. Wang Y, Klijn JG, Zhang Y, *et al*. Timmermans M, Meijer-van Gelder ME, Yu J et al.: Gene-expression profiles to predict distant metastasis of lymph-node-negative primary breast cancer. Lancet 2005, 365(9460):671-79.

31. Minn AJ, Gupta GP, Padua D, *et al*. Lung metastasis genes couple breast tumor size and metastatic spread. Proc Natl Acad Sci U S A 2007, 104(16):6740-6745.

32. Sotiriou C, Wirapati P, Loi S, *et al*. Gene expression profiling in breast cancer: understanding the molecular basis of histologic grade to improve prognosis. J Natl Cancer Inst 2006, 98(4):262-72.

33. Desmedt C, Piette F, Loi S, *et al*. Strong time dependence of the 76-gene prognostic signature for node-negative breast cancer patients in the TRANSBIG multicenter independent validation series. Clin Cancer Res 2007, 13(11):3207-14.

34. Schmidt M, Böhm D, Von Törne C, *et al*. The humoral immune system has a key prognostic impact in node-negative breast cancer. Cancer Res 2008, 68(13):5405-13.

35. Riaz M, van Jaarsveld MT, Hollestelle A, *et al*. miRNA expression profiling of 51 human breast cancer cell lines reveals subtype and driver mutation-specific miRNAs. Breast Cancer Res 2013, 15(2):R33.

36. Calon A, Espinet E, Palomo-Ponce S, *et al*. Dependency of colorectal cancer on a TGFβ-driven program in stromal cells for metastasis initiation. Cancer Cell 2012, 22(5):571-584.

37. McCall MN, Bolstad BM, Irizarry RA. Frozen robust multiarray analysis (fRMA). Biostatistics 2010, 11(2):242-53.

38. Johnson WE, Li C, Rabinovic A. Adjusting batch effects in microarray expression data using empirical Bayes methods. Biostatistics 2007, 8(1):118-27.

39. Martens JW, Sieuwerts AM, Bolt-deVries J, *et al*. Aging of stromal-derived human breast fibroblasts might contribute to breast cancer progression. Thromb Haemost 2003, 89(2):393-404.

40. Ramkisoensing AA, Pijnappels DA, Askar SF, *et al*. Human embryonic and fetal mesenchymal stem cells differentiate toward three different cardiac lineages in contrast to their adult counterparts. PLoS One 2011, 6(9):e24164.

41. Ren J, Liu S, Cui C, *et al*. Invasive Behavior of Human Breast Cancer Cells in Embryonic Zebrafish. J Vis Exp 2017(122):e55459.

42. Dennler S, Itoh S, Vivien D, t *et al*. Direct binding of Smad3 and Smad4 to critical TGFβ-inducible elements in the promoter of human plasminogen activator inhibitor-type 1 gene. EMBO J 1998, 17(11):3091-100.

43. Persson U, Izumi H, Souchelnytskyi S, *et al*. The L45 loop in type I receptors for TGF-β family members is a critical determinant in specifying Smad isoform activation. FEBS Lett 1998, 434(1-2):83-87.

44. Krause C, Kloen P, ten Dijke P. Elevated transforming growth factor β and mitogen-activated protein kinase pathways mediate fibrotic traits of Dupuytren's disease fibroblasts. Fibrogenesis Tissue Repair 2011, 4(1):14.

**3**

45. Naber HP, Wiercinska E, ten Dijke P, *et al*. Spheroid assay to measure TGFβ-induced invasion. J Vis Exp 2011(57) :e3337.

46. Buijs J, Van Der Horst G, Van Den Hoogen C, *et al*. The BMP2/7 heterodimer inhibits the human breast cancer stem cell subpopulation and bone metastases formation. Oncogene 2012, 31(17):2164-74.

47. Vogt J, Traynor R, Sapkota GP. The specificities of small molecule inhibitors of the TGFβ and BMP pathways. Cell Signal 2011, 23(11):1831-42.

48. Karnoub AE, Dash AB, Vo AP, *et al*. Mesenchymal stem cells within tumour stroma promote breast cancer metastasis. Nature 2007, 449(7162):557-63.

49. Chen MH, Yeh YC, Shyr YM, *et al*. Expression of gremlin 1 correlates with increased angiogenesis and progression-free survival in patients with pancreatic neuroendocrine tumors. 2013 J Gastroenterol, 48(1):101-8.

50. Jang BG, Kim HS, Chang WY, *et al*. Prognostic significance of stromal GREM1 expression in colorectal cancer. Hum Pathol 2017, 62:56-65.

51. Sato M, Kawana K, Fujimoto A, *et al*. Clinical significance of Gremlin 1 in cervical cancer and its effects on cancer stem cell maintenance. Oncol Rep 2016, 35(1):391-7.

52. Grivennikov SI, Greten FR, Karin MJC. Immunity, inflammation, and cancer. 2010, 140(6):883-9.

53. Hawinkels LJ, ten Dijke P. Exploring anti-TGFβ therapies in cancer and fibrosis. Growth factors 2011, 29(4):140-52.

54. Guan Y, Cheng W, Zou C, *et al*. Gremlin1 promotes carcinogenesis of glioma in vitro. Clin Exp Pharmacol Physiol 2017, 44(2):244-56.

55. Yin M, Tissari M, Tamminen J, *et al*. Gremlin-1 is a key regulator of the invasive cell phenotype in mesothelioma. Oncotarget 2017, 8(58):98280-97.

56. Ravelli C, Mitola S, Corsini M, *et al*. Involvement of α v β 3 integrin in gremlin-induced angiogenesis. Angiogenesis 2013, 16(1):235-43.

57. Lavoz C, Alique M, Rodrigues-Diez R, *et al*. Gremlin regulates renal inflammation via the vascular endothelial growth factor receptor 2 pathway. J Pathol 2015, 236(4):407-20.

58. Ciuclan L, Sheppard K, Dong L, *et al*. Treatment with Anti–Gremlin 1 Antibody Ameliorates Chronic Hypoxia/SU5416–Induced Pulmonary Arterial Hypertension in Mice. Am J Pathol 2013, 183(5):1461-73.

59. Song K, Krause C, Shi S, *et al*. Identification of a key residue mediating bone morphogenetic protein (BMP)-6 resistance to noggin inhibition allows for engineered BMPs with superior agonist activity. 2010, 285(16):12169-80.

60. Sugimoto H, LeBleu VS, Bosukonda D, *et al*. Activin-like kinase 3 is important for kidney regeneration and reversal of fibrosis. Nat Med 2012, 18(3):396-404.

61. Shin K, Lim A, Zhao C, *et al*. Hedgehog signaling restrains bladder cancer progression by eliciting stromal production of urothelial differentiation factors. Cancer Cell 2014, 26(4):521-33.

3

Supplementary Table 1. **Quantitative real-time PCR Primers**

Genes		Sequence (5' to 3')
ACTA2	Forward	CTGTTCCAGCCATCCTTCATC
	Reverse	CCGTGATCTCCTTCTGCATT
ACVR2A	Forward	GCATCACAAGATGGCCTACC
	Reverse	CCAGGCAAACTGTAGACTTC
ACVR2B	Forward	ATGTGGACATCCATGAGGAC
	Reverse	TGAAGATCTCCCGTTCACTC
ALK1	Forward	CTGGTTCCGGGAGACTGAGAT
	Reverse	TGCGGGAGGTCATGTCTGA
ALK2	Forward	TGCCTTCGAATAGTGCTGTC
	Reverse	CATCAAGCTGATTGGTGCTC
ALK3	Forward	GGGGTCCGGACTTATGAAA
	Reverse	TACGACTCCTCCAAGATGTGG
ALK4	Forward	GCTCGAAGATGCAATTCTGG
	Reverse	TTGGCATACCAACACTCTCG
ALK6	Forward	CTTGCTGTATTGCTGACCTG
	Reverse	TCAGCCATGATGTAAGACTGG
ALK7	Forward	CGCACTTCAAAAGGGTGTCG
	Reverse	TGATGCCCAACATGCTCCTT
BMP2	Forward	GCAGGCACTCAGGTCAG
	Reverse	ATTCGGTGATGGAAACTGC
BMP4	Forward	TGTCTCCCCGATGGGATTCCCG
	Reverse	AATGGCTCCATAGGTCCCTGCAGTA
BMP6	Forward	CACCCAAGGGCTATGCTGCCAATTA
	Reverse	AGGTGAACCAAGGTCTGCACAATCG
BMP7	Forward	GTGCACTCGAGCTTCATCCA
	Reverse	GATCCGATTCCCTGCCCAAG
BMP15	Forward	AGAACCCGACAAGCAGATGG
	Reverse	AATGGCGTGATTGGGGGAAT
BMPR2	Forward	AACTGTTGGAGCTGATTGGC
	Reverse	CGGTTTGCAAAGGAAAACAC
COL1A1	Forward	CAGCCGCTTCACCTACAGC
	Reverse	TTTGTATTCAATCACTGTCTTGCC
COL1A2	Forward	GGCCCTCAAGGTTTCCAAGG
	Reverse	CACCCTGTGGTCCAACAACTC
FAP	Forward	CAATGTGGTACTCTGACCAGAACC
	Reverse	TCTGATACAGGCTTGCATCTGC
FN1	Forward	CGTCATAGTGGAGGCACTGA
	Reverse	CAGACATTCGTTCCCACTCA
GAPDH	Forward	TGCACCACCAACTGCTTAGC
	Reverse	GGCATGGACTGTGGTCATGAG

|		
GDF2	Forward	GACGTCCGATAAGTCGACTACGC
	Reverse	AAGATGTGCTTCTGGAAGGGGAA
GREM1	Forward	ACAGTCGCACCATCATCAAC
	Reverse	TAGTGAATTTCTTGGGCTTG
ID1	Forward	CTGCTCTACGACATGAACGG
	Reverse	GAAGGTCCCTGATGTAGTCGAT
ID3	Forward	CACCTCCAGAACGCAGGTGCTG
	Reverse	AGGGCGAAGTTGGGGCCCAT
MMP3	Forward	TGGATGCCGCATATGAAG
	Reverse	CAGAAATGGCTGCATCGA
MMP7	Forward	ACTTCAGGCAGAACATCCAT
	Reverse	ATTGCTAAATGGAGTGGAGG
MMP8	Forward	CTGTATCCACTTTCAGAATGTT
	Reverse	TACAGTGATGGGAAACAATGA
MMP9	Forward	TACTGTGCCTTTGAGTCCG
	Reverse	TTGTCGGCGATAAGGAAG
NCAD	Forward	CAGACCGACCCAAACAGCAAC
	Reverse	GCAGCAACAGTAAGGACAAACATC
PAI1	Forward	CACAAATCAGACGGCAGCACT
	Reverse	CATCGGGCGTGGTGAACTC
OCT4	Forward	CGAGAAGGATGTGGTCCGAG
	Reverse	AGCCTGGGGTACCAAAATGG
S100A4	Forward	TCTTTCTTGGTTTGATCCTGACT
	Reverse	AGTTCTGACTTGTTGAGCTTGA
SLUG	Forward	ATGAGGAATCTGGCTGCTGT
	Reverse	CAGGAGAAAATGCCTTTGGA
SNAI1	Forward	GCTGCAGGACTCTAATCCAGAGTT
	Reverse	GACAGAGTCCCAGATGAGCATTG
SOX2	Forward	CGGAAAACCAAGACGCTCAT
	Reverse	TGTGCGCGTAACTGTCCAT
TAZ	Forward	CCCGGCCGGAGAGTACAT
	Reverse	GACTGGTGATTGGACACGGT
TGFB2	Forward	GTGCTCTGTGGGTACCTTGA
	Reverse	GCGCTGGGTTGGAGATGTTA
TGFB3	Forward	CTGGCCCTGCTGAACTTTG
	Reverse	AAGGTGGTGCAAGTGGACAGA
VIM	Forward	CCAAACTTTTCCTCCCTGAACC
	Reverse	CGTGATGCTGAGAAGTTTCGTTGA
YAP	Forward	CGGCAGGCAATGCGGAATATCAAT
	Reverse	ACCATCCTGCTCCAGTGTTGGTAA
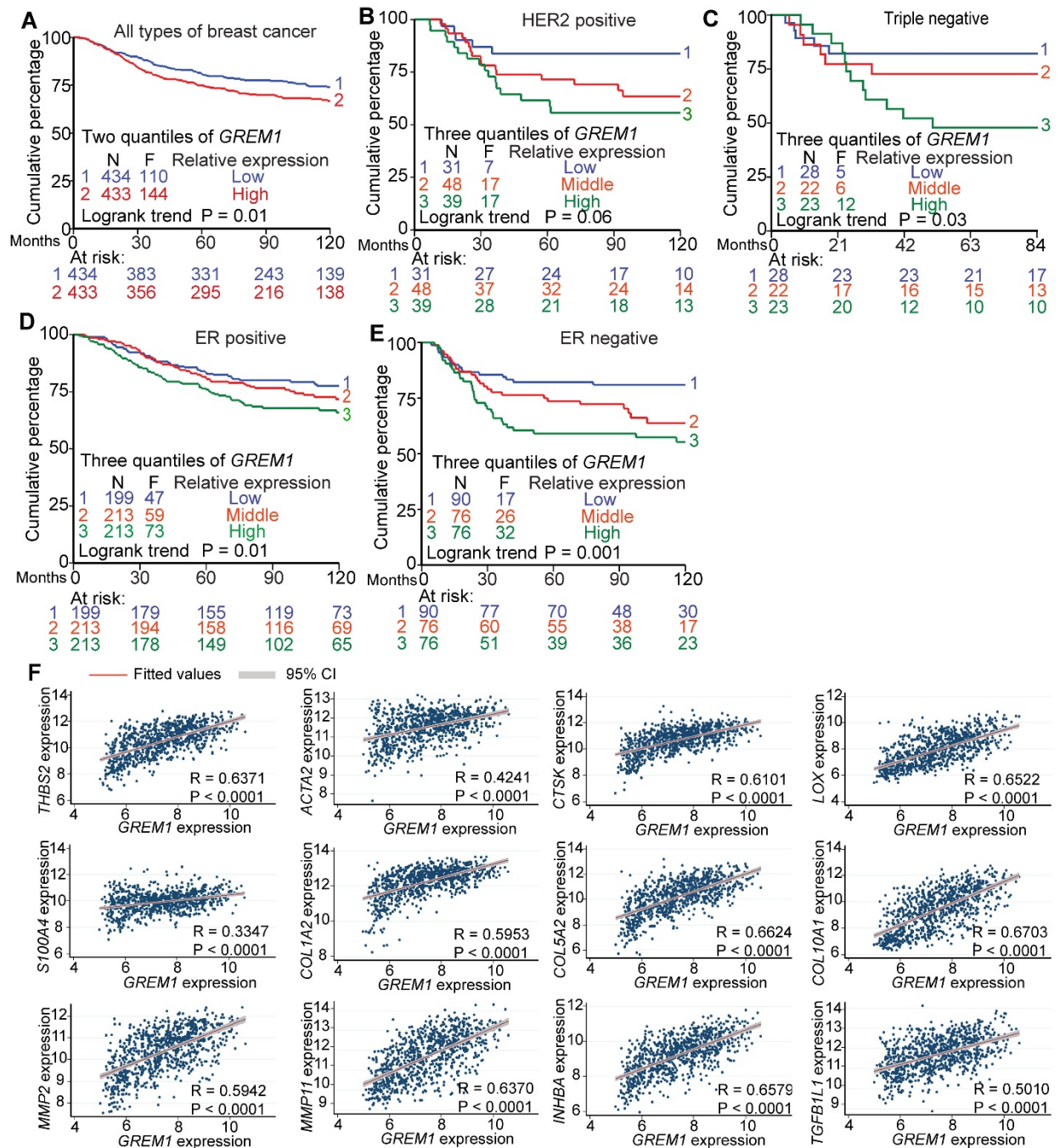
Supplementary Figure 1, **related to Figure 1. A**, Kaplan-Meier analysis of metastasis free survival based on GREM1 expression. Endpoint is distant metastasis free survival (MFS). **B-E**, Kaplan-Meier survival analysis of different breast cancer molecular subtypes, HER2^{+} (**B**), Triple[-] (**C**), ER[+] (**D**), and ER[-] (**E**). The subjects were divided into 3 quantiles. Endpoint is distant MFS. **F**, Scatterplot showing the positive correlation between *GREM1* and stromal genes / desmoplastic markers expression in clinical datasets. Pearson's coefficient tests were performed to assess statistical significance.
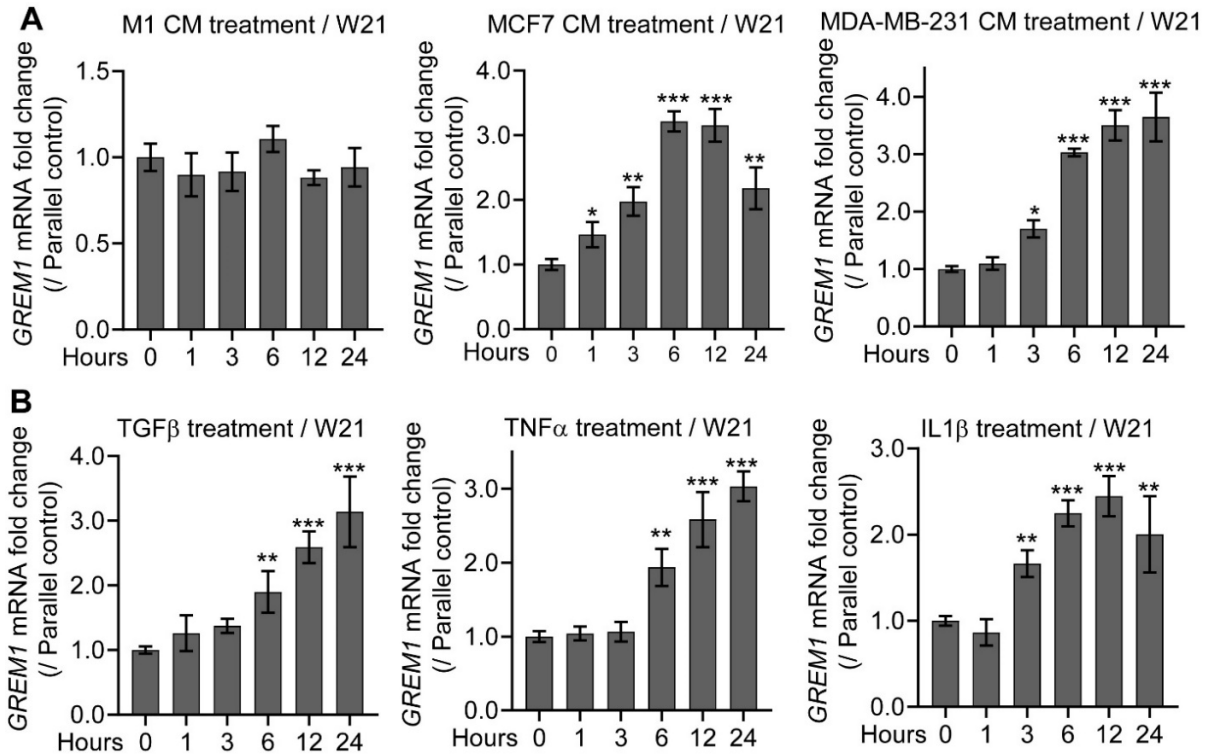
Supplementary Figure 2, related to Figure 2. A, *GREM1* expression in W21 MSCs after treatment with conditioned medium (CM) from breast cell lines (M1, MDA-MB-21, MCF7). Expression was normalized to the parallel time control of normal medium treatment. The results are expressed as the mean ± s.d, n = 3. Student's t test, *$P < 0.05$, ***$P \leq 0.001$. **B**, TGFβ3 (5 ng/ml), or TNFα (10 ng/ml), or IL1β (10 ng/ml) induces *GREM1* expression in W21 mesenchymal stem cells (MSCs). Expression was normalized to the parallel time control of buffer treatment. The results are expressed as the mean ± s.d., n = 3. Student's t test, *$P < 0.05$, **$P \leq 0.01$, ***$P \leq 0.001$.
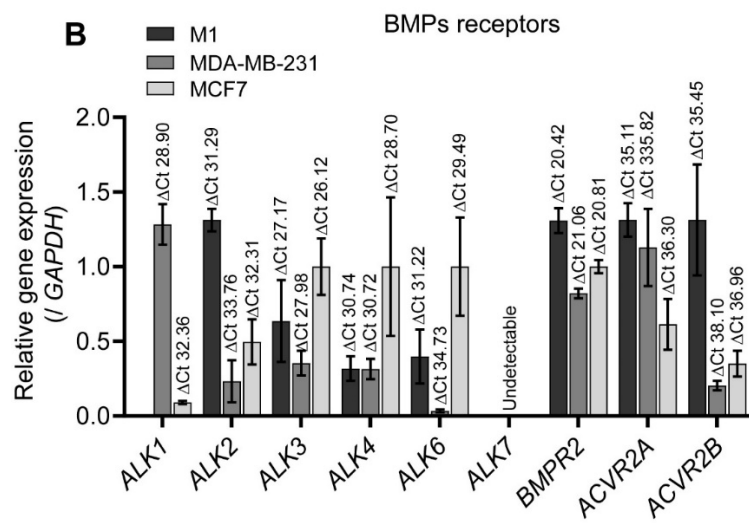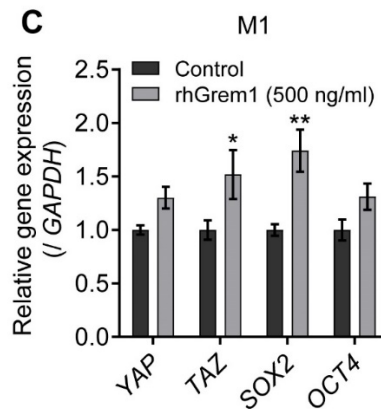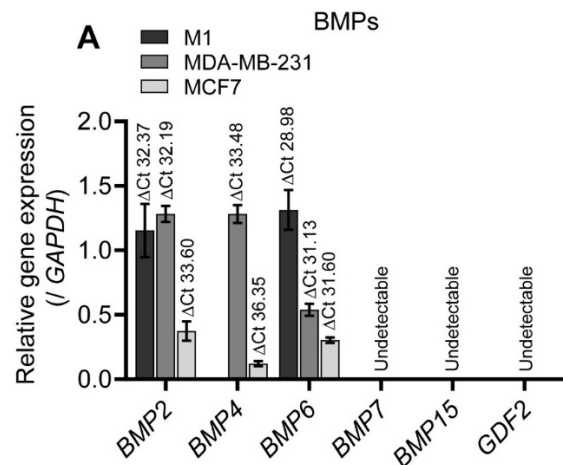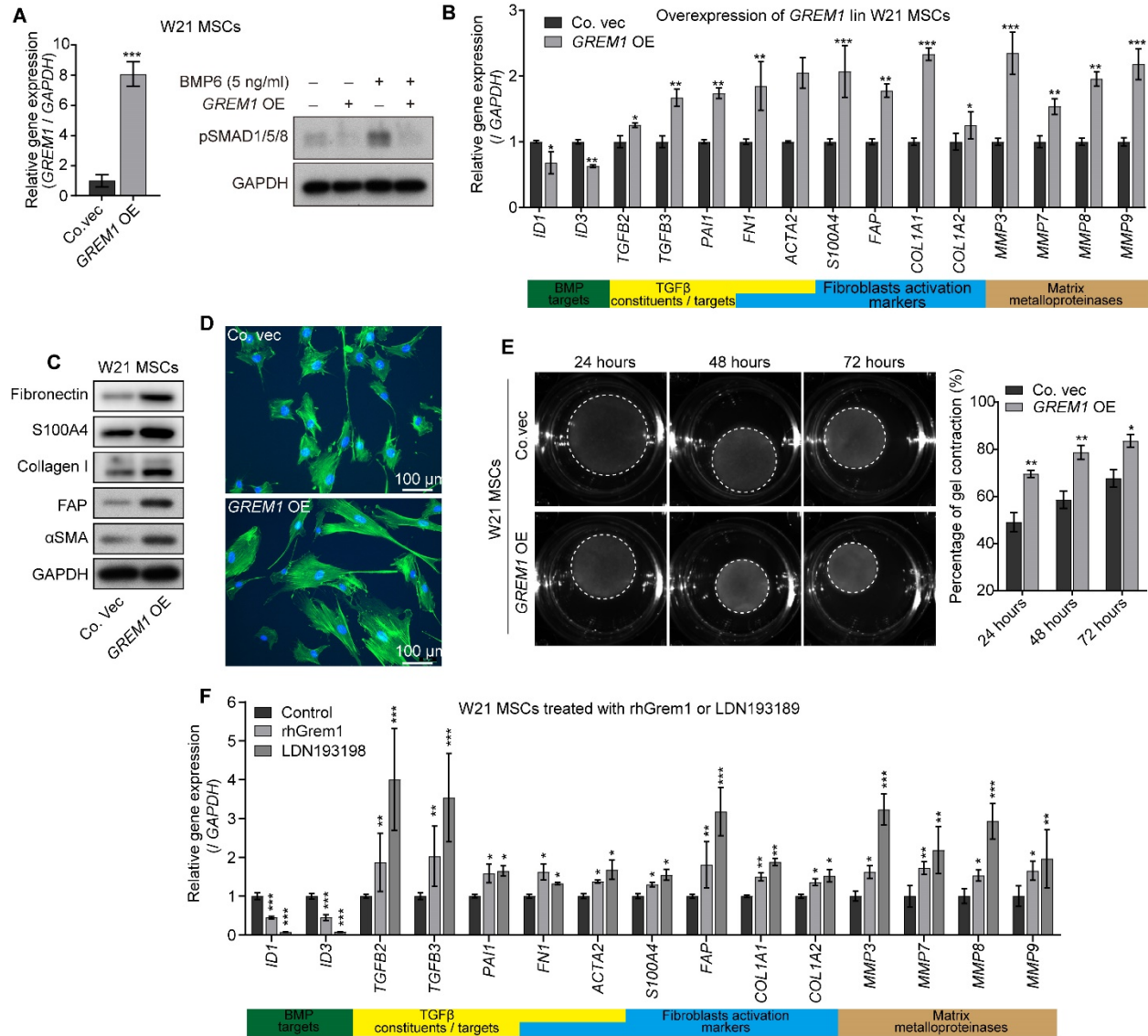
Supplementary Figure 3, related to Figure 3. A, B, qRT-PCR measurement for BMPs and BMP receptors in M1, MDA-MB-231 and MCF7 cell lines. ΔCt values are labeled to show expression abundance. **c** rhGrem1 upregulates stem cell transcription factors in M1 cells. *GAPDH* was used as an internal control. The results are expressed as the mean ± s.d., n = 3. Student's t test, *P < 0.05, **P ≤ 0.01.
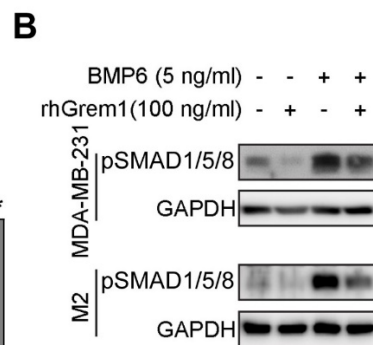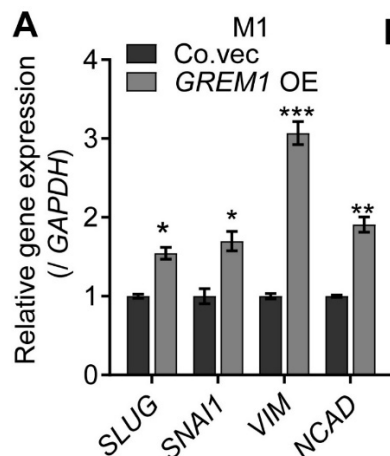

Supplementary 4, related to Figure 4. A, *GREM1* OE upregulates the expression of EMT transcription factors and markers in M1 cells. *GAPDH* was used as an internal control. The results are expressed as the mean ± s.d., n = 3. Student's t test, *P < 0.05, **P ≤ 0.01, ***P ≤ 0.001. **B,** exogenous administration of rhGrem1 inhibits BMP-induced SMAD1/5/8 phosphorylation (pSMAD1/5/8) in MDA-MB-231 and M2 cell lines.
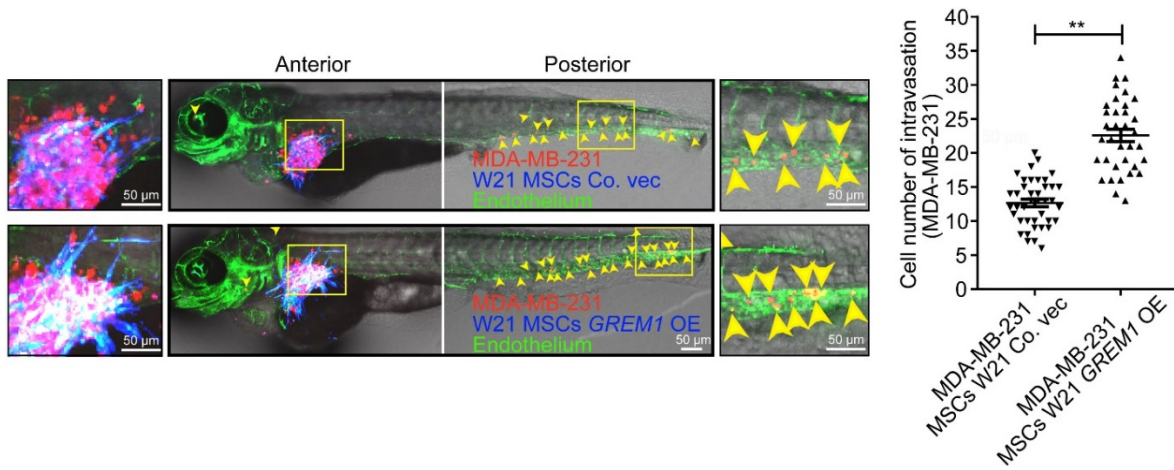
Supplementary Figure 5, related to Figure 5. *GREM1* overexpression (OE) in fetal mesenchymal stem cells (MSCs) W21 shows fibroblast-like characteristics. A, Stable *GREM1* OE in MSCs W21 inhibits BMP6 (5 ng/ml) induced SMAD1/5/8 phosphorylation (pSMAD1/5/8). Left, relative mRNA level determined by qRT-PCR. *GAPDH* was used as internal control. The results are expressed as the mean ± s.d., n = 3. Student's t test, ***P ≤ 0.001. **B**, qRT-PCR analysis of selected BMP targets, TGF pathway constituents/targets, fibroblasts activation markers, matrix metalloproteinases, in W21 MSCs with/without *GREM1* stable OE. *GAPDH* was used as internal control. The results are expressed as the mean ± s.d., n = 3. Student's t test, *P < 0.05, **P ≤ 0.01, ***P ≤ 0.001. **C**, Western blot to detect indicated proteins level change after *GREM1* OE in W21 MSCs. **D**, W21 MSCs with/without *GREM1* OE were stained with fluorescein-phalloidin (green) to visualize F-actin. DAPI was used for nuclear staining (blue). **E**, Collagen gel contraction assay. W21 MSCs with/without *GREM1* OE were embedded in

collagen gels. After 24, 48, and 72 h, the area of each gel (white dash circle) was imaged and quantified. Left, representative images of contracted gels. Right, percentage of gel contraction gel. Quantification is shown in Methods. The results are expressed as the mean ± s.d., n = 3. Student's t test, *$P < 0.05$, **$P \leq 0.01$. **F**, qRT-PCR analysis of selected genes in W21 MSCs after 48 hours treatment with recombinant human Grem1 (rhGrem1) protein (500 ng/ml) or BMP type I receptors inhibitor LDN193198 (120 nM). *GAPDH* was used as internal control. The results are expressed as the mean ± s.d., n = 3. Student's t test, *$P < 0.05$, **$P \leq 0.01$, ***$P \leq 0.001$.
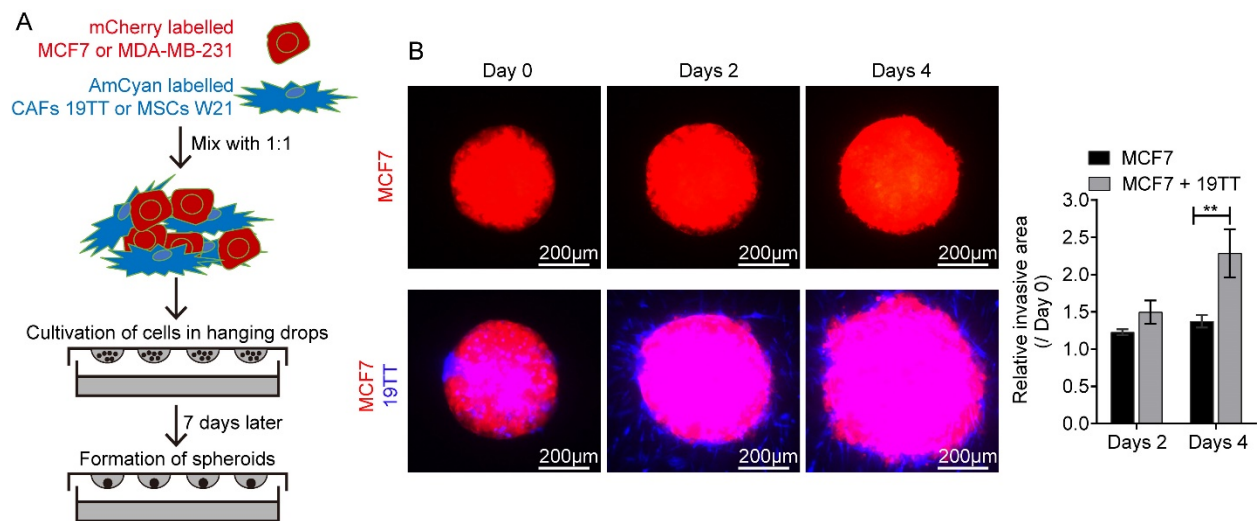
Supplementary Figure 6, related to Figure 6. Spheroid invasion assays. A, Schematic illustration of spheroid production. Briefly, mCherry-labeled MDA-MB-231 or MCF7 cells (Red) were mixed with AmCyan (converted to blue)-labeled 19TT breast cancer-associated fibroblasts (CAFs) at a ratio of 1:1. Mixtures were cultured for 7 days in hanging drops to obtain spheroids. **B**, 19TT CAFs promotes MCF7 cells invasion. Left, representative images of spheroids at days 0, 2, and 4. Red, MCF7 cells; Blue, 19TT CAFs. Right, the relative invasion area was quantified as area difference at days 2 and 4, relative to day 0. The results are expressed as the as the mean ± s.d., n = 8. Student's t test, **$P \leq 0.01$.

Supplementary Figure 7, related to Figure 7. *GREM1* overexpression (OE) in W21 mesenchymal stem cells (MSCs) promotes breast cancer cells intravasation in zebrafish embryo perivitelline space coinjection model. Perivitelline space co-injection of MDA-MB-231 cells and W21 MSCs with/without *GREM1* stable OE. The panels show representative images. Green, endothelium of zebrafish; Red, mCherry-labelled MDA-MB-231; Blue, converted from AmCyan-labelled W21. Yellow arrowheads point to single intravasated cells in the head and tail regions of zebrafish. Left, cells migration in the perivitelline space; middle, image of zebrafish embryo body; Right, visualization of intravasated cells in the posterior of embryo. The graph shows quantification of the number of intravasated cells in each embryonic body at 3 days post injection (dpi). The results are expressed as the mean ± s.e.m., n=2. Student's t test, **$P \leq 0.01$.

107
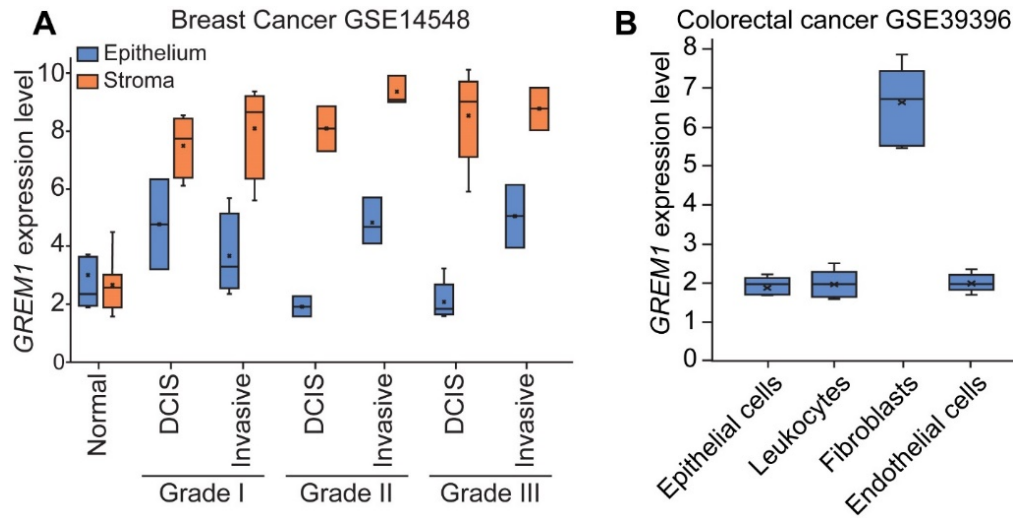
Supplementary Figure 8, related to Figure 1. A, *GREM1* mRNA expression in epithelium and stroma compartments in breast cancer dataset *GSE14548*. Epithelium and stroma were extracted from normal breast, grade I, II, III ductal carcinoma *in situ* (DCIS) and invasive breast cancer tissue using laser capture. **B**, *GREM1* expression in epithelial cells, leukocytes, fibroblasts and endothelial cells in colorectal cancer dataset *GSE39396*. Each specific type of cells were isolated by flow cytometry.